JOURNAL OF GEOPHYSICAL RESEARCH, VOL. 114, A06219, doi:10.1029/2008JA013855, 2009

Source locations of narrowband radio emissions detected at Saturn

Sheng-Yi Ye,[1] D. A. Gurnett,[1] G. Fischer,[1,2] B. Cecconi,[3] J. D. Menietti,[1] W. S. Kurth,[1] Z. Wang,[1] G. B. Hospodarsky,[1] P. Zarka,[3] and A. Lecacheux[3]

Received 27 October 2008; revised 31 March 2009; accepted 8 April 2009; published 24 June 2009.

[1] Since Cassini's arrival at Saturn in 2004, the Radio and Plasma Wave Science instrument has detected numerous narrowband (NB) radio emission events. These emissions, mostly detected around 5 and 20 kHz, usually occur periodically for several days after intensifications of Saturn kilometric radiation. We present calculations based on an electron density profile of Saturn's plasma torus and a dipole magnetic field model showing that the NB emissions originate from the northern and southern edges of Saturn's plasma torus at L shells $\sim$ 8 to 10 for 5-kHz NB and $L \sim 4$ to 7 for 20-kHz NB. In many cases, Cassini passes through the source region of the 20-kHz NB, as indicated by intense electrostatic upper hybrid (ESUH) waves in close proximity to electromagnetic emissions on spectrograms. The positions of the spacecraft when intense ESUH waves are observed agree with the model predictions of the NB source locations. Source locations determined by goniopolarimetric (also known as direction-finding) analysis of the NB emissions also support the above results, although sometimes the directions of arrival point toward the region interior to Saturn's plasma torus. A polarization reversal technique is applied to localize the NB emissions observed during spacecraft rotation, on the basis of the fact that the source is within the antenna plane when the apparent circular polarization degree switches sign. The NB emissions are found to be L-O mode polarized, which is consistent with the prediction of linear/nonlinear mode conversion theory. It is also found that sometimes right-hand polarized NB emissions are generated at second harmonic frequencies of the 20-kHz NB; in which case, wave-wave interactions between oppositely propagating ESUH waves may play an important role in the mode conversion process.

Citation: Ye, S.-Y., D. A. Gurnett, G. Fischer, B. Cecconi, J. D. Menietti, W. S. Kurth, Z. Wang, G. B. Hospodarsky, P. Zarka, and A. Lecacheux (2009), Source locations of narrowband radio emissions detected at Saturn, *J. Geophys. Res.*, *114*, A06219, doi:10.1029/2008JA013855.

1. Introduction

[2] Planetary radio emissions induced by nonthermal plasmas can be categorized into two types on the basis of their generation mechanism: (1) directly generated emissions, like the intense auroral radio emissions generated in the Earth's auroral regions by the cyclotron maser instability [*Gurnett*, 1974; *Wu and Lee*, 1979], and (2) mode-converted emissions, like terrestrial continuum and narrowband radio emissions, which are believed to be generated via mode conversion from electrostatic waves [*Gurnett*, 1975; *Jones*, 1976; *Melrose*, 1981]. Like the directly generated auroral radio emissions, the narrowband radio emissions are present at all five radio planets of the solar system and are also found to be emitted by the Jovian moon, Ganymede [*Kurth et al.*, 1997]. The characteristics of nonthermal continuum (NTC) radiation, Jovian narrowband kilometric radiation (n-KOM) and narrowband emissions from other outer planets are similar to each other, and they are believed to be generated by the same type of mechanism: mode conversion from electrostatic upper hybrid bands, most likely in regions with steep density gradients [*Gurnett and Shaw*, 1973; *Frankel*, 1973; *Gurnett*, 1975; *Shaw and Gurnett*, 1975; *Jones*, 1976; *Kurth*, 1982; *Fung and Papadopoulos*, 1987; *Jones*, 1988; *Kurth*, 1992; *Reiner et al.*, 1993; *Menietti et al.*, 2003, 2005a, 2005b].

[3] Detections of narrowband radio emission at Saturn date back to the Voyager era, when the Voyager 1 and 2 Plasma Wave Science (PWS) instruments observed a series of narrowband emissions at frequencies between 3 and 30 kHz originating from the inner region of the magnetosphere [*Gurnett et al.*, 1981; *Scarf et al.*, 1982]. Voyager 1 PWS wideband spectrograms obtained over a 3-day period (Voyager 1 traveled from 3.26 R_S (Saturn radii) to 58.3 R_S within this period) revealed a persistent band of emission around 5 kHz, providing the best evidence that the 5 kHz emission is a freely propagating electromagnetic wave.

[1]Department of Physics and Astronomy, University of Iowa, Iowa City, USA.
[2]Space Research Institute, Austrian Academy of Sciences, Graz, Austria.
[3]Observatoire de Paris, Meudon, France.

0148-0227/09/2008JA013855$09.00

Observations near the source (when the spacecraft was close to the planet and passing through the plasma disk) showed that the narrowband emissions are observed only in the low-density regions outside of the plasma sheet where the wave frequency is greater than the local electron plasma frequency, $f > f_{pe}$. The emission had a sharp low-frequency cutoff, which was attributed to f_{pe}, and it extended across the local electron cyclotron frequency f_{ce} without obvious propagation changes; these characteristics led to the interpretation that the narrowband emission was propagating in the L-O mode, although Voyager PWS used only one dipole antenna, hence, no direct observations of the polarization of narrowband emissions were available. Examination of the spectrograms also showed evidence of a periodic modulation of the narrowband emission intensities at the rotation period of Saturn [*Gurnett et al.*, 1981; *Scarf et al.*, 1982].

[4] Twenty-four years after the Voyager spacecraft flew by Saturn, the Cassini spacecraft was inserted into orbit around Saturn on 1 July 2004. Since then, narrowband emissions have been frequently detected by the Radio and Plasma Wave Science (RPWS) instrument [*Gurnett et al.*, 2004, 2005]. During orbit insertion, RPWS detected a large number of narrowband emissions in the frequency range from 3 to 70 kHz in the region over the rings, similar to the free space L-O mode narrowband radio emissions observed by Voyager 1 and 2 at Saturn. In a further investigation of the emissions observed during orbit insertion, *Farrell et al.* [2005] argued that the narrowband emissions detected between 3 and 70 kHz within planetocentric distances of less than 2.5 R_S were Z mode waves generated by mode conversion from f_{pe} electrostatic waves on steep density gradients parallel to the magnetic field vector **B**. Since the Z mode is not a free space mode [e.g., *Gurnett and Bhattacharjee*, 2005], these waves cannot escape from the plasma disk and thus cannot be observed at great distance from the planet. In order for these Z mode waves to be observed by a spacecraft located in Saturn's outer magnetosphere, a second mode conversion from Z to L-O mode is necessary [*Jones*, 1976; *Melrose*, 1981; *Budden and Jones*, 1987].

[5] Recently, *Louarn et al.* [2007] associated the occurrence of narrowband radio emissions at 5 kHz with "energetic events" in Saturn's magnetosphere, as indicated by intensifications of Saturn kilometric radiation (SKR). They found that the sources of these 5-kHz narrowband radio emissions, or n-SMR (narrowband Saturn Myriametric Radiation) in their terminology, corotate and sometimes even supercorotate with the planet. It was also found that these emissions were more easily detected after an energetic event, if the spacecraft is at low latitudes. On the basis of the analogy between Jovian n-KOM and n-SMR, they assumed O mode propagation for n-SMR, which means n-SMR can only exist in low-density regions. *Louarn et al.* [2007] then considered the possibility that the sources of narrowband emissions are in the inner ($L \sim 2$) or outer ($L \sim 10$ to 12) region of the plasma disk near the equatorial plane. *Louarn et al.* [2007] also pointed out that for a source in the inner part of the plasma disk to be observable at lower latitudes outside the plasma disk, a significant plasma evacuation from the external layers of the disk is required.

[6] Z. Wang et al. (Narrowband radio emissions and their relationship to rotating plasma clouds and magnetic disturbances at Saturn, submitted to *Journal of Geophysical Research*, 2008) summarized the observations of narrowband radio emissions since Cassini's orbit insertion in 2004 and examined the possible association of the narrowband radio emissions with a rotating plasma cloud detected by MIMI/INCA (Magnetospheric IMaging Instrument/Ion and Neutral Camera) onboard Cassini [*Krimigis et al.*, 2004]. Rotational modulation tests show that the narrowband radio emissions act like a clock rather than a rotating beacon. This means that a change in local time of the spacecraft does not change the measured period, whereas the period of a rotating beacon (e.g., light house beam) would be changed when the observer changes its position. They also found that less intense emissions at frequencies $\geq$20 kHz (otherwise called n-SKR by *Lamy et al.* [2008]) were only observable at higher latitudes. High-resolution wideband waveform data from RPWS revealed a fine structure of the 5-kHz narrowband emissions and showed that the emissions consist of multiple subbands whose intensities are modulated at a period of $\sim$10–20 min. No modulation of such timescales, however, could be observed in the $\geq$20 kHz narrowband radio emissions detected.

[7] This paper focuses on the source location of narrowband radio emissions detected at Saturn. Section 2 describes a theoretical model of the source locations of Kronian narrowband radio emissions. Section 3 shows a pass through the source of the narrowband emission observed by Cassini/RPWS. The coordinates of the spacecraft in the source region are compared to the model predictions. Section 4 discusses the polarization of the narrowband emissions. Section 5 discusses the Cassini goniopolarimetric measurements. Section 6 shows the tests of the source location model using the goniopolarimetric (direction-finding) results. In section 7, a polarization reversal technique is implemented to locate the plane that contains the source of the narrowband emissions.

2. Model for the Source Location of Narrowband Emissions

[8] The narrowband radio emissions are believed to be first excited as electrostatic waves when the matching condition $f_{UH} = (n + 1/2)f_{ce}$ is met, where $f_{UH} = \sqrt{f_{pe}^2 + f_{ce}^2}$ is the upper hybrid frequency, f_{ce} is the electron cyclotron frequency and n is the harmonic number [*Ashour-Abdalla and Kennel*, 1978; *Rönnmark*, 1978; *Kurth et al.*, 1979a, 1981; *Kurth*, 1982; *Yoon et al.*, 1996, 1998]. $(n + 1/2)f_{ce}$ emissions is a general term for emissions that occur between nf_{ce} and $(n + 1)f_{ce}$, and the exact frequency is dependent on plasma conditions, including the density and temperature of a warm plasma [e.g., *LaBelle et al.*, 1999; *Benson et al.*, 2001].

[9] Electrostatic $(n + 1/2)f_{ce}$ waves near f_{UH} are frequently observed in space plasmas and are often found to be associated with observations of loss cone electron distributions at the source [*Kurth et al.*, 1979b]. Theoretical studies by *Rönnmark* [1978] based on simultaneous measurements of electrostatic $(n + 1/2)f_{ce}$ waves and the electron distribution function indicate that a hot loss cone component of the electron distribution function can account for the wave growth around $(n + 1/2)f_{ce}$ with the growth rate maximizing when $(n + 1/2)f_{ce} \cong f_{UH}$ because of the nonconvective nature of the instability.

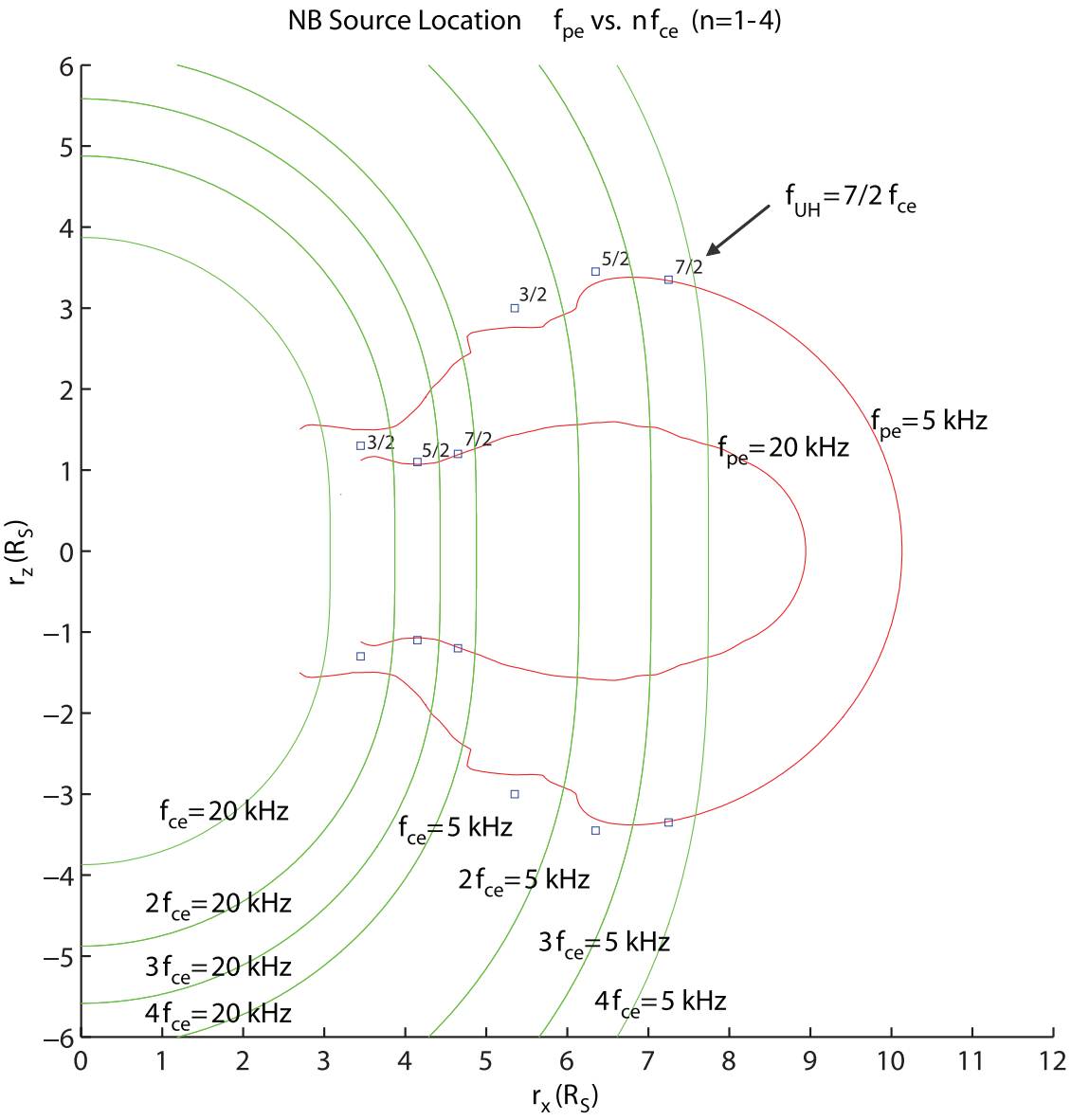

Figure 1. A model of the source location of narrowband emissions based on a scale height density model of Saturn's plasma torus [*Persoon et al.*, 2006] and a dipole magnetic field model [*Ness et al.*, 1981]. The green contour lines stand for constant f_{ce} surfaces, and the red curves in the plot are f_{pe} contours for 5 and 20 kHz. The squares near the f_{pe} contours and between two adjacent f_{ce} contour lines mark the source locations of the 5-kHz and the 20-kHz narrowband emissions.

[10] *Ashour-Abdalla and Kennel* [1978] explored parameter space while computing the wave growth in a plasma consisting of a hot and a cold component with a weak loss cone distribution. They found that the ratio between the upper hybrid frequency (determined from the cold electron density) and the electron cyclotron frequency f_{UH}/f_{ce} determines the number of possible $(n + 1/2)f_{ce}$ bands between f_{ce} and f_{UH} whereas the ratio between cold and hot plasma density n_C/n_H determines which of the $(n + 1/2)f_{ce}$ bands should be excited. The ratio between cold and hot plasma temperature T_C/T_H controls the nonconvective or convective nature of the instability. This was confirmed by *Hubbard and Birmingham* [1978], and they give a summary of the parametric study in their Table 2. The simulation results are consistent with the Cassini/RPWS observation where $(n + 1/2)f_{ce}$ waves are frequently observed in low-density regions near f_{UH} when f_{UH} is comparable to f_{ce}. As Cassini enters the plasma torus ($2-10R_S$ and low latitudes), the cold plasma density increases and f_{UH} becomes much greater than f_{ce}, the low-$(n + 1/2)f_{ce}$ waves disappear and only upper hybrid bands are observed.

[11] To model the source location of narrowband emissions, we numerically calculated the locations where the matching condition $(n + 1/2)f_{ce} \cong f_{UH}$ is met in a meridian plane (Figure 1), using the scale height electron density model given by *Persoon et al.* [2006] and a dipole magnetic field model [*Ness et al.*, 1981]. The electron density model of the plasma torus is based on 116,000 electron densities derived from measurements of upper hybrid frequencies over a range of L shell, $3.6 \leq L \leq 8.6$, and latitudes, $-20°$

Table 1. Model Results for Narrowband Source Locations

Frequency (kHz)	n	Radial Distance (R_S)	L Shell	Latitude (deg)
5	1	6.1	8.1	29.3
5	2	7.2	9.4	28.5
5	3	8.0	9.7	24.8
20	1	3.7	4.2	20.6
20	2	4.3	4.6	14.8
20	3	4.8	5.1	14.5
20	4	5.2	5.6	15.0
20	5	5.6	6.0	15.0
20	6	5.9	6.3	15.2

to +16°. Outside this region, there are few electron density measurements because of either spacecraft trajectory limitations or the intensity of the upper hybrid emissions falling below background noise levels. Thus the contour lines represented by $f_{pe} = 5$ *kHz* in Figure 1 are an extrapolation of the data used in the *Persoon et al.* [2006] model. On the basis of fittings of the measurements during the first 17 orbits, the density model of the plasma torus assumes local time and longitudinal symmetry. Likewise, the dipole magnetic field model given by *Ness et al.* [1981] is axisymmetric.

[12] For a certain frequency f, the source location of narrowband emissions is assumed to be near the $f_{UH} = f$ and the $(n + 1/2)f_{ce} = f$ contours. In Figure 1, the green contour lines are constant f_{ce} surfaces, where $nf_{ce} = 5$ kHz and 20 kHz ($n = 1, 2, 3, 4$). Note that the $4f_{ce} = 20$ kHz and $f_{ce} = 5$ kHz contour lines coincide. The red curves in the plot are f_{pe} contours for 5 and 20 kHz. The squares near the f_{pe} contour ($f_{UH} \sim f_{pe}$ when $n > 1$) and between two adjacent f_{ce} contour lines mark the theoretical source locations of the 5-kHz and the 20-kHz narrowband emissions, with three solutions for each frequency corresponding to $f_{UH} = 3/2f_{ce}$, $f_{UH} = 5/2f_{ce}$ and $f_{UH} = 7/2f_{ce}$, respectively. The modeled source locations of narrowband emissions are listed in Table 1. Note that the source locations of the 20-kHz narrowband emissions are generally closer to Saturn and at lower latitudes compared to those of the 5-kHz narrowband emissions. As the n value increases the predicted source locations for a certain frequency move away from Saturn along a constant density surface of the plasma torus.

[13] Wang et al. (submitted manuscript, 2008) showed that the 20-kHz narrowband emissions are mainly observed when Cassini is at high latitudes. In Figure 1, the modeled source locations of the 20-kHz narrowband emissions are on the inner side of the plasma torus, which means that L-O mode emissions originated from these locations would be refracted by the torus to higher latitudes, so that the 20-kHz narrowband emissions cannot be observed when Cassini is at lower latitudes outside the plasma torus. On the other hand, the 5-kHz narrowband emissions with higher harmonic numbers can be observed by Cassini on the equatorial plane outside of the plasma torus, because their propagation paths are not blocked by the plasma torus.

3. Cassini's Encounters With the Narrowband Emission Source

[14] During its many orbits around Saturn, Cassini went through the plasma torus on almost every orbit. This region can be identified in the dynamic spectrum by strong electrostatic upper hybrid (ESUH) waves. One can easily notice that the frequency and bandwidth of the narrowband emissions are similar to those of the intensified ESUH waves on the spectrograms. It is believed that these electrostatic waves can mode convert to electromagnetic narrowband emissions in regions of steep plasma density gradients, i.e., on the edges of the plasma torus [*Gurnett et al.*, 1981]. This mode conversion process could be either via a linear [*Jones*, 1976] or a nonlinear [*Melrose*, 1981] mechanism.

[15] In many cases Cassini went through the source region of narrowband emissions, as indicated by a strong electrostatic wave immediately preceding or following the radio emission. Figure 2a shows a dynamic spectra of the RPWS data for day of year (DOY) 003, 2008. The horizontal axis is marked with spacecraft event time (SCET) and spacecraft coordinates. The vertical axis shows the frequency in Hz. The intensity of the emissions are color coded so that red stands for signal intensities 35 dB above the background noise level. In this spectrogram, the upper hybrid resonance frequency (f_{UH}) and the electron cyclotron frequency (f_{ce}), marked by a white curve, satisfy the matching condition $f_{UH}(22.4\ \text{kHz}) \cong 11/2\ f_{ce}$ (4.0 kHz) around 1856 SCET, when ESUH waves are intensified. This intensification of ESUH waves is preceded by an observation of emissions, believed to be electromagnetic, between 1600 and 1856 SCET. These emissions are most likely electromagnetic because their frequencies are independent of the local parameters f_{ce} and f_{pe}. Similarly, the emission around 1730 SCET also represents a match of $(n + 1/2)f_{ce}$ and f_{UH}. In this case, $n = 4$ and is preceded by narrowband radio emissions. The enhanced emissions near 1930 SCET, on the other hand, are not accompanied by electromagnetic narrowband emissions. These emissions correspond to a match of $(n + 1/2)f_{ce}$ and f_{UH} with $n = 6$. Similar observations of the source of escaping terrestrial continuum radiation have been shown by *Kurth* [1982].

[16] Figure 2b compares the position of Cassini to the modeled source location for the time interval when intensified ESUH waves are observed (1800–1856 SCET). The black curve in Figure 2b illustrates the spacecraft trajectory. The source locations are calculated on the basis of frequencies of the ESUH waves and local f_{ce} ($n = 5$) using the method described above. We assume an axisymmetric plasma torus, hence the source locations displayed as points in the meridional plots of Figure 1 are actually ring shaped sources. The possible sources of the narrowband emissions form a pair of rings around Saturn, one in the northern and one in the southern hemisphere as shown in Figure 2c, which is a view from the direction that is perpendicular to the spacecraft meridian. In Figure 2b, only the northern hemisphere rings can be seen in the top view. The two red rings are the modeled source locations for two different frequencies between 19 and 25 kHz, corresponding to two selected channels of the RPWS High Frequency Receiver (HFR). It is clear that the trajectory of the spacecraft is very close to the modeled source rings. Similar agreement is found in many other events. The model provides a good prediction of where the intensified ESUH waves might occur within the plasma torus of Saturn. Examples like that shown in Figure 2 occur during many periapsis passes. Table 2 lists the narrowband source encounters recorded by Cassini since Saturn orbit insertion (SOI). These source

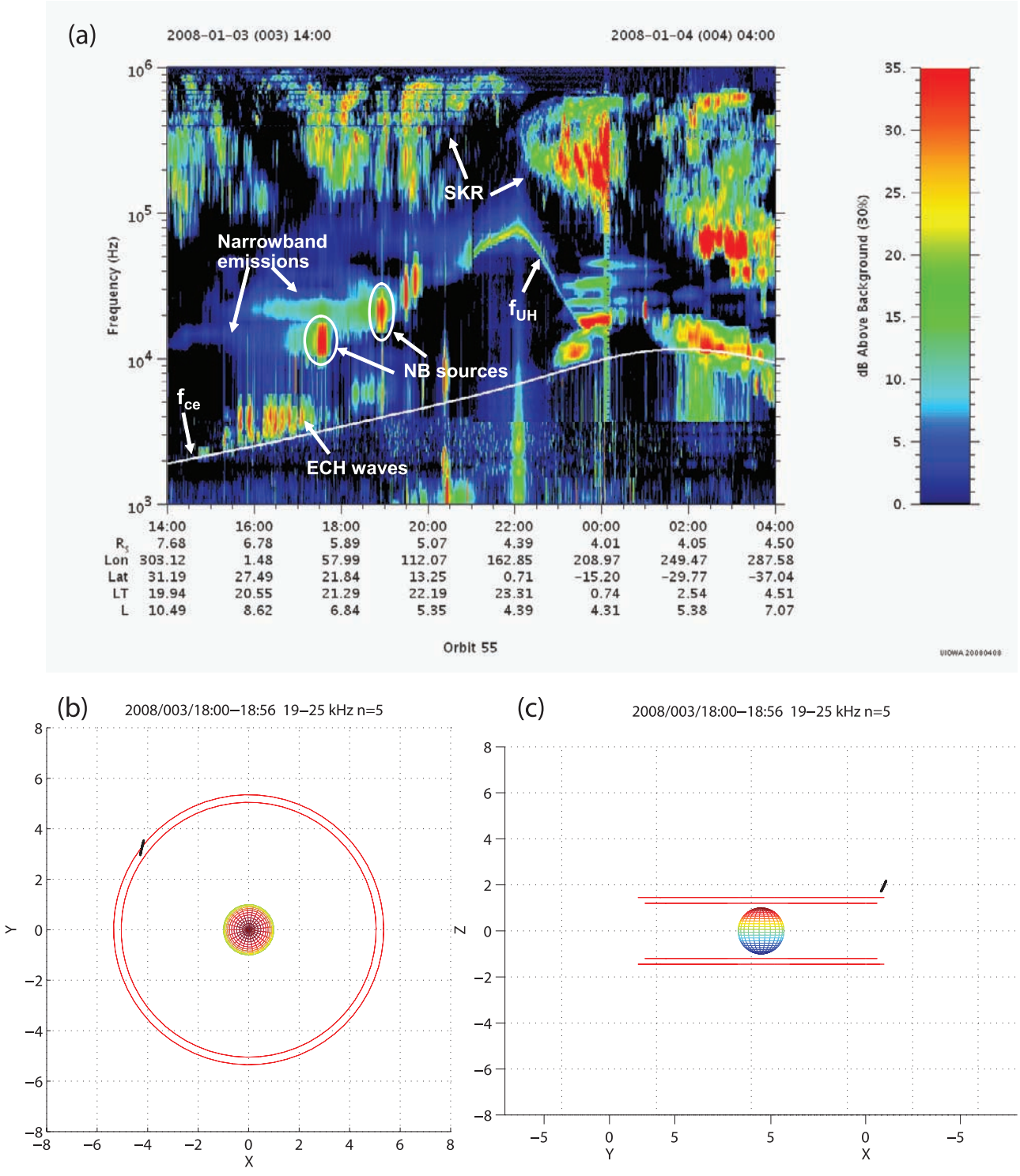

Figure 2. Source passing of a 20-kHz narrowband emission. (a) A dynamic spectrum of the RPWS data of DOY 003, 2008. The matching condition f_{UH}(22.4 kHz) ≅ 11/2 f_{ce} (f_{ce} = 4.0 kHz) is satisfied around 1856 SCET, when the electrostatic upper hybrid (ESUH) waves are intensified. The intensified ESUH waves at 1856 SCET are the source of the electromagnetic waves that precede them. The color bar shows the intensity above the background, and for each frequency channel the background level of 0 dB (black color) is set at the 30% occurrence level of the intensity histogram. (b)A top view and (c) a side view of the comparison between the modeled source ring and the Cassini trajectory when the intense ESUH waves are observed.

Table 2. The 20-kHz Narrowband Source Encounter Events

Year-DOY	Time (SCET)	Frequency (kHz)	*n*	LT
2005-141	0600	17	1	20
2005-159	1000	20	1	19
2005-177	1600	20	1	20
2005-195	2200	24	2	20
2005-214	0500	14	1	18
2005-232	1130	20	1	20
2006-229	0735	15	12	17
2006-269	0330	11	3	16
2007-114	1820	11	3	3
2007-130	2240	21	2	3
2007-130	2345	15	1	4
2007-147	0000	21	1	3
2007-163	0040	34	1	3
2008-003	1733	12	3	21
2008-003	1856	22	5	21
2008-015	2150	20	1	0
2008-027	1955	20	1	0
2008-062	0336	30	3	23
2008-062	0350	22	2	23
2008-121	1300	19	2	0
2008-146	2250	20	1	23

crossing events strongly support the mode conversion theory of at least the 20-kHz narrowband emissions.

4. Polarization of Narrowband Emission

[17] The linear mode conversion theory [*Jones*, 1976] predicts that the terrestrial continuum radiation should be emitted in the L-O mode. This prediction was later tested and confirmed by *Gurnett et al.* [1988]. At Saturn, the polarization of narrowband emissions can be measured by Cassini RPWS.

[18] When narrowband emissions are observed at high latitudes, we assume that the radio emission propagates in free space mode right after it leaves the source region and its polarization with respect to the wave vector **k** then remains the same in the absence of plasma effects [*Gurnett et al.*, 1988]. So the mode of propagation at the source can be determined on the basis of the polarization measurement at the spacecraft and the knowledge of the source location.

[19] Figure 3 illustrates the geometry when Cassini detects both SKR and narrowband radio emissions at high latitudes. Because $\mathbf{k} \cdot \mathbf{B} > 0$ for both SKR and narrowband emission in this situation, the measured polarization of these two emissions should be identical to the mode of propagation at the source. It has been shown that SKR is right-hand polarized with the spacecraft at northern latitudes [*Lamy et al.*, 2008; *Cecconi et al.*, 2009] and narrowband emission is generally left-hand polarized when observed from northern latitudes (G. Fischer et al., Real and apparent polarization of Saturn narrowband radio emissions, paper presented at *European Geosciences Union General Assembly 2008*, Vienna, 2008). So we conclude that the primary Saturn narrowband radio emission (5 kHz) is emitted in L-O mode, which is consistent with the mode conversion theory.

[20] It has also been shown that some of the higher-frequency narrowband emissions (>30 kHz) are polarized the same way as SKR [e.g., *Lamy et al.*, 2008, Figures 3 and 6]. As shown in Figure 1, the predicted source locations of higher-frequency narrowband emissions are closer to the equator, which makes the beaming angle (the angle between **k** and **B**; see Figure 3) exceed 90° when the observation point is at high latitude close to Saturn. This switches the sense of polarization as measured by the spacecraft, but with

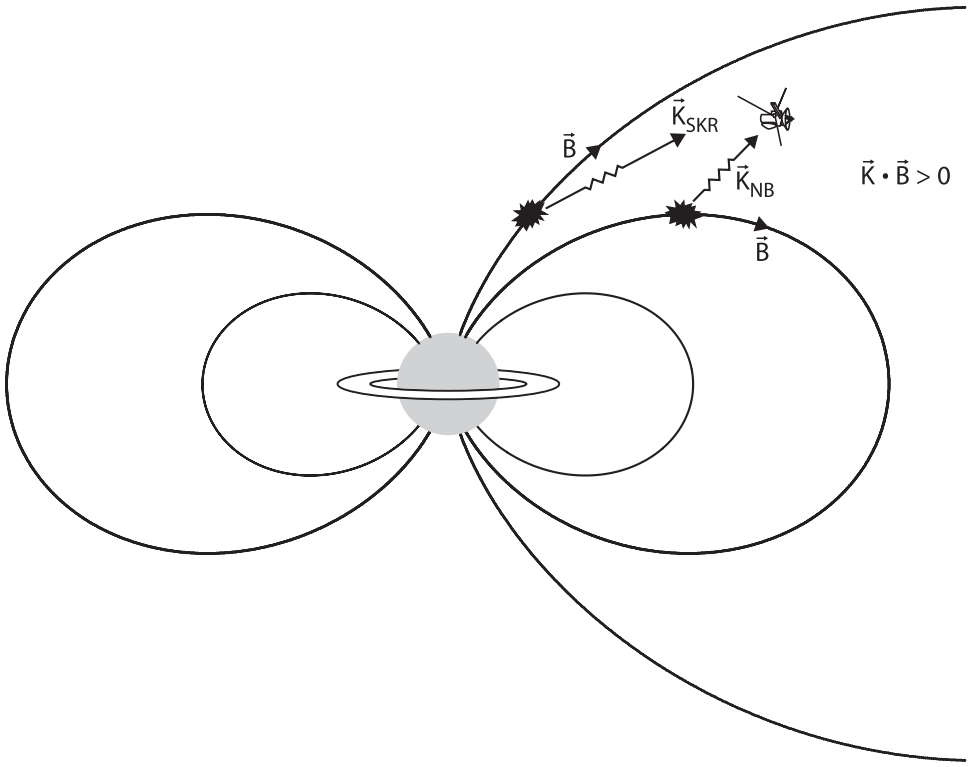

Figure 3. A typical geometry when Cassini detects both SKR and narrowband radio emissions at high latitudes.

respect to the **B** field at the source the narrowband emission is still emitted in the left-hand ordinary (L-O) mode. So if the narrowband emissions are all emitted in the L-O mode, then the polarization change at higher frequencies as observed by Cassini could be explained by the beaming angle crossing the 90° threshold.

5. Radio Goniopolarimetry

[21] Goniopolarimetry is a data analysis tool that allows us to retrieve the flux, polarization state and direction of arrival of an electromagnetic wave. Measurements by the three electric antennas (E_u, E_v, E_w) of the Cassini Radio and Plasma Wave Science (RPWS) instrument allow us to determine the direction of arrival, the Poynting flux (S) and the polarization of a plane wave (Stokes parameters Q, U, V) coming from a point radio source using the analytical inversion methods provided by A. Lecacheux (Two antenna direction finding with purely circular polarization, paper presented at Cassini/RPWS Team Meeting Presentation, University of Iowa, Iowa City, 2000) and *Cecconi and Zarka* [2005]. The RPWS/HFR can be operated in either two-antenna (dipole-monopole) mode (where E_u and E_v are used as a dipole E_x; 2 auto correlations of E_x and E_w and one complex cross correlation between E_x and E_w are measured), or three-antenna/direction-finding (DF) mode (where E_u and E_v are used as monopoles; two consecutive sets of auto and cross correlations are measured between E_u/E_v and E_w antennas).

[22] The goniopolarimetric inversion involves expressing the 6 wave parameters (S, Q, U, V, θ and ϕ) as functions of the antenna measurements (θ and ϕ are the colatitude and azimuth angle of the direction of arrival in the spacecraft frame) [*Cecconi and Zarka*, 2005]. Since in the often used two-antenna mode we have only 4 antenna measurements but 6 parameters to solve for in the equations, assumptions have to be made on the wave parameters. We thus assume no linear polarization (i.e., $Q = 0$ and $U = 0$). The narrowband emissions have been found to be purely circularly polarized at high latitudes but partially polarized or unpolarized at low latitudes with no linear component (Fischer et al., presented paper, 2008), which justifies the use of the two-antenna direction inversion at least at high latitudes. On the other hand, no assumption is necessary in the three-antenna (DF) mode direction inversion, because the number of measurements (7 independent measurements because the auto correlation of E_w is measured twice) exceeds the 6 unknown parameters. Therefore the three-antenna mode measurements allow us to characterize the full polarization as well as the direction of arrival of an incoming radio wave. The two-antenna mode can give the direction of arrival to the source, provided the polarization assumption is valid.

6. Testing the Source Location Model of Narrowband Emissions Using Goniopolarimetric Results

[23] The goniopolarimetric results and the modeled source locations of narrowband emissions are compared. In most of the events shown, only the two-antenna goniopolarimetric result is available, because, until now, Cassini/RPWS mainly operated in the dipole-monopole (i.e., two-antenna) mode because of its lower data rate, higher-frequency time resolution and higher signal-to-noise ratio on the dipole antenna. In one event, RPWS/HFR was operating in the three-antenna mode. For this event, the two-antenna goniopolarimetric inversion is applied to the data by treating each sample as two separate two-antenna measurements. Thus the results of the two goniopolarimetric inversions can be directly compared.

6.1. Data Selection

[24] In order to compare the theoretical model of narrowband emission source locations and the goniopolarimetric results, narrowband emissions with accurate direction-finding results need to be used. We select the narrowband emission events on the basis of the following criteria: (1) the signal-to-noise ratio (SNR) should be at least 23 dB and (2) the total degree of polarization should be greater than 0.8.

[25] Before the direction inversions are applied to the antenna measurements, a background level based on a long-term average is subtracted from the measurements. The background is computed as the 5% occurrence level of the histogram of auto correlation values (V^2/Hz) built from a series of 3 months of data, for each frequency setup of the receiver. This long-term determination has proved to be effective for the galactic background [*Zarka et al.*, 2004]. This background subtraction is satisfactory for SKR frequencies, since the background level is relatively homogeneous in that frequency range. However, for the frequency range of narrowband emissions, the background noise level is highly variable because of the variability of the plasma noise, impact noise and 1/f noise. The same background subtraction that works for SKR would introduce errors for narrowband emissions with low intensity levels. Nonetheless, the background subtraction will not affect intense narrowband emissions because, compared to their intensity levels, the background noise level is negligible. Therefore, we select relatively intense (> 23 dB) narrowband emissions for goniopolarimetry.

[26] A high degree of polarization is required for interpreting the goniopolarimetric data, because waves with a low degree of polarization do not have a well defined phase difference between two perpendicular components of the electric field vector. This leads to a significant scattering of the measurement values of the cross correlation which is translated to a significant scattering of incoming wave directions retrieved from the goniopolarimetric algorithm.

[27] According to *Cecconi and Zarka* [2005], for these selection criteria the accuracy of the direction of arrival is about 2°. This error mainly comes from the error of the antenna calibration and the digitization error. The error from the calibration would be a systematic one, whereas the digitization error is random. So the source locations calculated from the goniopolarimetric results would be less accurate as the distance between Cassini and the wave source increases. Narrowband emissions observed at low latitudes are excluded from the test because these narrowband emissions are found to be mostly unpolarized, which violates criterion 2.

[28] Caution is needed when interpreting the goniopolarimetric results for the narrowband emissions observed near perikrone, because (1) the waves observed close to the

planet are not propagating in the free space mode, implying the **E** plane normal is often not parallel to the wave vector, so that the goniopolarimetry applied to these waves yields a wrong direction of arrival; and (2) when the spacecraft is close to the narrowband emission source, the point source assumption may be questionable, and according to *Cecconi* [2007], any source with anglular size greater than 5° should be considered as an extended source. Also if Cassini is too far from Saturn, then the waves observed might not be strong enough to overcome the background.

[29] Because of the factors discussed above, we choose narrowband emission events observed at relatively high latitudes, around 8–20 R_S from Saturn, to compare with the model. From 2004 to 2008, Cassini RPWS captured plenty of narrowband emissions that meet these criteria.

6.2. Testing the Model Using Two-Antenna Goniopolarimetry

[30] It would have been ideal to use three-antenna goniopolarimetry for the comparison with the model, since the two-antenna goniopolarimetry is based on the zero linear polarization assumption. However, the availability of three-antenna goniopolarimetric results is limited because most of the time, the HFR is operating in the two-antenna mode. In this subsection, we apply the two-antenna goniopolarimetry to narrowband emission events observed at high latitudes and medium distance from Saturn. The source location derived from the goniopolarimetric results are compared to that predicted by the model. The first two events shown are 5 kHz narrowband emissions and the last event is a 20 kHz narrowband emission.

6.2.1. Case 1

[31] Figure 4a shows the spectrogram of a 5-kHz narrowband radio emission event that lasted from 1600 to 2000 SCET on DOY 081, 2008. Figures 4b–4e show the goniopolarimetric results for the limited time range of 1800 to 1900 SCET. This restricted interval was selected to reduce the scatter in the distributions as a result of a slight change in spacecraft attitude during the entire 1600–2000 SCET interval. The HFR was operating in dipole-monopole mode. The imaginary parts of the cross correlation measurements between the dipole E_x and the monopole E_w, $Im(X)$ (processed directly on the spacecraft), the circular polarization degree (V), θ and ϕ of the direction of arrival are plotted against the signal-to-noise ratios of the dipole X axis antenna (SNR_{autoX}) in Figures 4b–4e. The circular polarization degrees of the waves corresponding to the data points with $SNR_{autoX} > 23$ dB are ~ 1 as shown in Figure 4c. And the direction of arrival parameters (θ and ϕ) also converge with increasing signal-to-noise values as shown in Figures 4d and 4e. Cassini was at $\sim 47°$ latitude and ~ 18 R_S from Saturn when this narrowband emission was observed.

[32] We determine the 3-D position for the source by computing the intersection of the direction of arrival with the plane containing the modeled source rings, like those shown in Figure 2 and choosing the ring in the same hemisphere as the spacecraft. The other ring is not a likely source because the low-frequency waves could not propagate through the plasma disk. In order to find the 3-D location of the narrowband emission source, we assume that the radio emission propagates in a straight line between the source and the spacecraft. Note that this assumption might not always be valid. For example, when Cassini is at low latitude, narrowband emissions can be refracted by the plasma torus. However, when Cassini is at high latitude, this refraction effect is negligible because of the low plasma density at high latitudes. Thus, it is reasonable to assume a straight line propagation path for the narrowband emissions observed at high latitudes. Figure 5a shows the 3-D location for the narrowband emission source described above. The black diamonds on the top right corner mark the Cassini trajectory. The red rings represent the modeled source locations of narrowband emissions for frequencies between 3 and 8 kHz. The locations of these rings are calculated on the basis of $n = 1$ in the matching condition. Assuming straight line propagation, we intersect the directions of arrival with the plane containing the source rings. The resulting intersection points are shown as magenta dots. Each of these intersection points corresponds to a set of 4 measurements by the HFR in the frequency range of 3 to 8 kHz between 1800 and 1900 SCET.

[33] In Figure 5a, all measurement points with signal-to-noise ratio $SNR_{autoX} > 23$ dB are treated equally as magenta dots. To better illustrate the source localization, we create contour plots of the source locations taking into account the intensity level of each set of measurements. First, the plane containing the modeled source ring is divided into 1 $R_S \times 1$ R_S (R_S = 60,268 km) cells. Then, all SNR_{autoX} (in dB) associated with the source locations within each cell are summed to create a matrix of numbers of all cells from which we build a contour plot. A 4-h-long narrowband emission, observed between 1600 and 2000 SCET, is divided into $\sim$ 7-min intervals. For each of the intervals, a contour plot of source locations is produced and these contour plots are combined into a movie, which can be found in the auxiliary material (Movie S1).[1] A frame of the movie is shown in Figure 5b. It should be noted that in the 4-h-long movie, the source location of the narrowband emission does not rotate with the planet, but is fixed in local time. Also the determined source location of the narrowband emission is not within the meridian plane of the spacecraft. This video clearly shows that the source regions cluster around the predicted source locations. The color bar on the right-hand side of the movie shows the intensity levels of the contour lines with red contour lines corresponding to 300 accumulated dB. These red contour lines represent the most probable source locations of the narrowband emissions for the reason we discussed above: the goniopolarimetric results are more accurate for intense and highly polarized waves.

6.2.2. Case 2

[34] Figure 6a shows a spectrogram with a $\sim$5-h-long 5-kHz narrowband emission. Each of the intersection points shown in Figure 6b corresponds to the 3-D source location for the narrowband emission observed from 2200 to 2300 SCET of DOY 363, 2006. The HFR was operating in dipole-monopole mode. The spacecraft was at $\sim -33°$ latitude and ~ 14 R_S from Saturn when this narrowband emission was observed. Each of these intersection points corresponds to a set of 4 measurements by HFR in the frequency range of 3 to 8 kHz between 2200 and 2300 SCET. It should be noted

[1] Auxiliary materials are available in the HTML. doi:10.1029/2008JA013855.

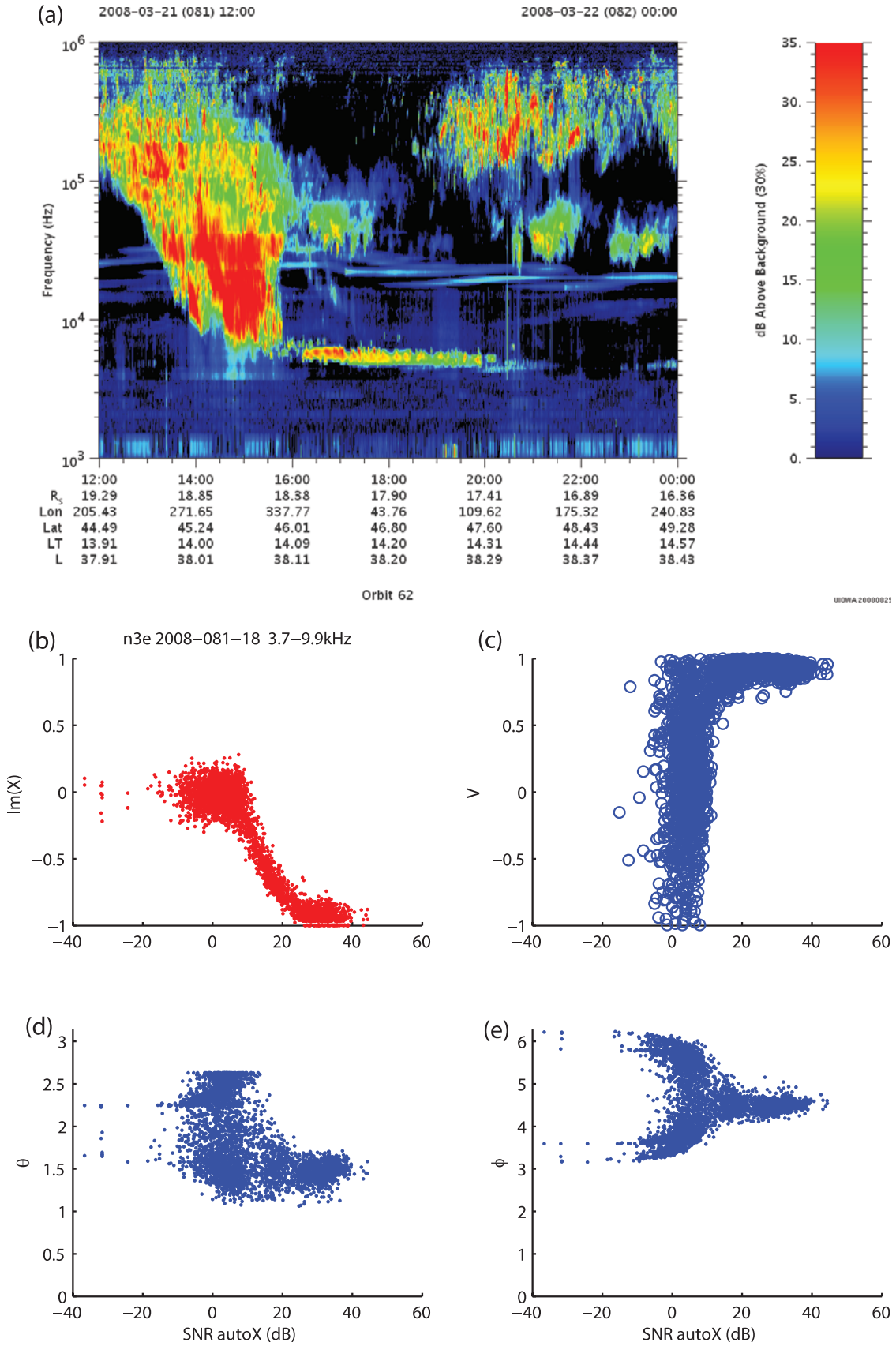
(a)
2008-03-21 (081) 12:00
2008-03-22 (082) 00:00
Frequency (Hz)
dB Above Background (30%)
12:00 14:00 16:00 18:00 20:00 22:00 00:00
R_S 19.29 18.85 18.38 17.90 17.41 16.89 16.36
Lon 205.43 271.65 337.77 43.76 109.62 175.32 240.83
Lat 44.49 45.24 46.01 46.80 47.60 48.43 49.28
LT 13.91 14.00 14.09 14.20 14.31 14.44 14.57
L 37.91 38.01 38.11 38.20 38.29 38.37 38.43
Orbit 62
(b)
n3e 2008–081–18 3.7–9.9kHz
Im(X)
(c)
V
(d)
θ
SNR autoX (dB)
(e)
ϕ
SNR autoX (dB)

Figure 4

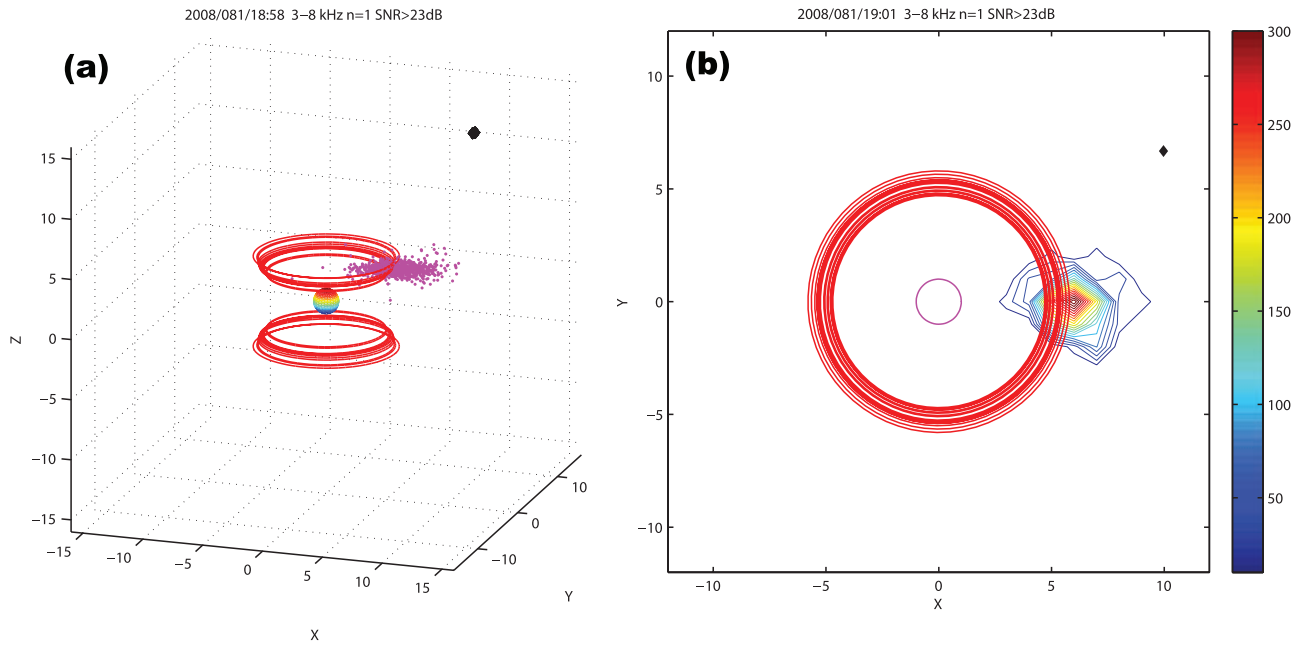

Figure 5. (a) The 3-D source location of the 5-kHz narrowband emission observed by Cassini/RPWS from 1800 to 1900 SCET of DOY 081, 2008. The black diamonds on the top right corner mark the Cassini trajectory. The red rings represent the modeled source locations of narrowband emissions for frequencies between 3 and 8 kHz. The locations of these rings are calculated on the basis of $n = 1$ in the matching condition. Assuming no propagation effects between the source and the spacecraft, the intersections of the directions of arrival with the plane containing the source rings, magenta points, are the source locations of the narrowband emission. (b) A frame of Movie S1 showing the contour of weighted narrowband source locations determined from direction-finding results.

that the source is in the southern hemisphere. Movie S2 shows the source locations for narrowband emissions observed between 2000 and 2400 SCET of DOY 363, 2006. In this event, the source location of the narrowband emission again does not rotate with the planet, but is fixed in local time.

6.2.3. Case 3

[35] A top view of the 3-D source location of the 20-kHz narrowband emission observed from 0500 to 0600 SCET of DOY 213, 2005 is shown in Figure 7b. Cassini was at $\sim -22^\circ$ latitude and $\sim 14\ R_S$ from Saturn. The HFR was operating in the dipole-monopole mode. In this case, the source locations determined from the goniopolarimetric results matches the modeled source ring corresponding to a harmonic number $n = 6$. (Note: the actual observed emission frequency is used in the calculations rather than 20 kHz.) The faint blue rings correspond to $n = 1$. It should be noted that the determined source is not within the meridian plane of the spacecraft. For case 1 (see Figure 5b), the determined source is also not within the meridian plane.

6.3. Comparison of Two-Antenna and Three-Antenna Goniopolarimetric Results

[36] To validate the two-antenna goniopolarimetric assumptions, we compare the modeled source location of a 5-kHz narrowband emission to both the two-antenna and the three-antenna goniopolarimetric results. The emission used for this comparison was observed between 1100 and 1900 SCET of DOY 120, 2008, as shown in Figure 8a. During the first 3 h of this event, the HFR was operating in dipole-monopole mode (two-antenna mode). Starting at 1400 SCET, the HFR switched to three-antenna mode. Both goniopolarimetric inversion methods can be applied to the three-antenna mode data, making the comparison between the two methods possible.

[37] Figure 8b shows a contour plot of the source locations of the narrowband emission derived from the three-antenna goniopolarimetry results. The source locations appear to extend across the region enclosed by the modeled source ring. This seems to indicate that the real source locations are located at higher latitudes than we modeled, which is possible since the density contour line corresponding to the 5 kHz plasma frequency is an extrapolated one. In Figure 8c, the two-antenna goniopolarimetric inversion is applied to the three-antenna mode data, and the contour plot of the resulting narrowband source locations are shown. The results of these two methods are basically consistent with each other, although in both results, the directions of arrival point away from the modeled source ring toward the center. The possible causes are (1) as stated before, the observed waves are not propagating in free space mode, so the measured

Figure 4. (top) Dynamic spectrum and (bottom) the two-antenna goniopolarimetric results for a 5 kHz narrowband emission observed by Cassini/RPWS from 1800 to 1900 SCET of DOY 081, 2008 (Figure 4a). (b) The imaginary parts of the cross correlation measurements ($Im(X)$) between the dipole E_x and the monopole E_w, (c) the circular polarization degree (V), (V), (d) θ and (e) ϕ of the direction of arrival are plotted against the signal-to-noise ratios of the dipole antenna (SNR_{autoX}).

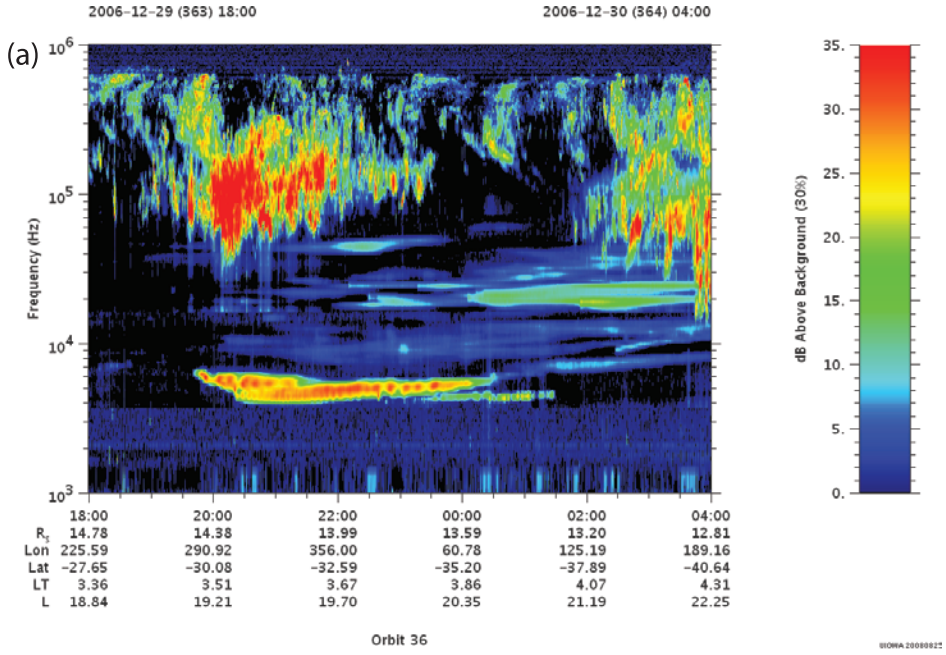

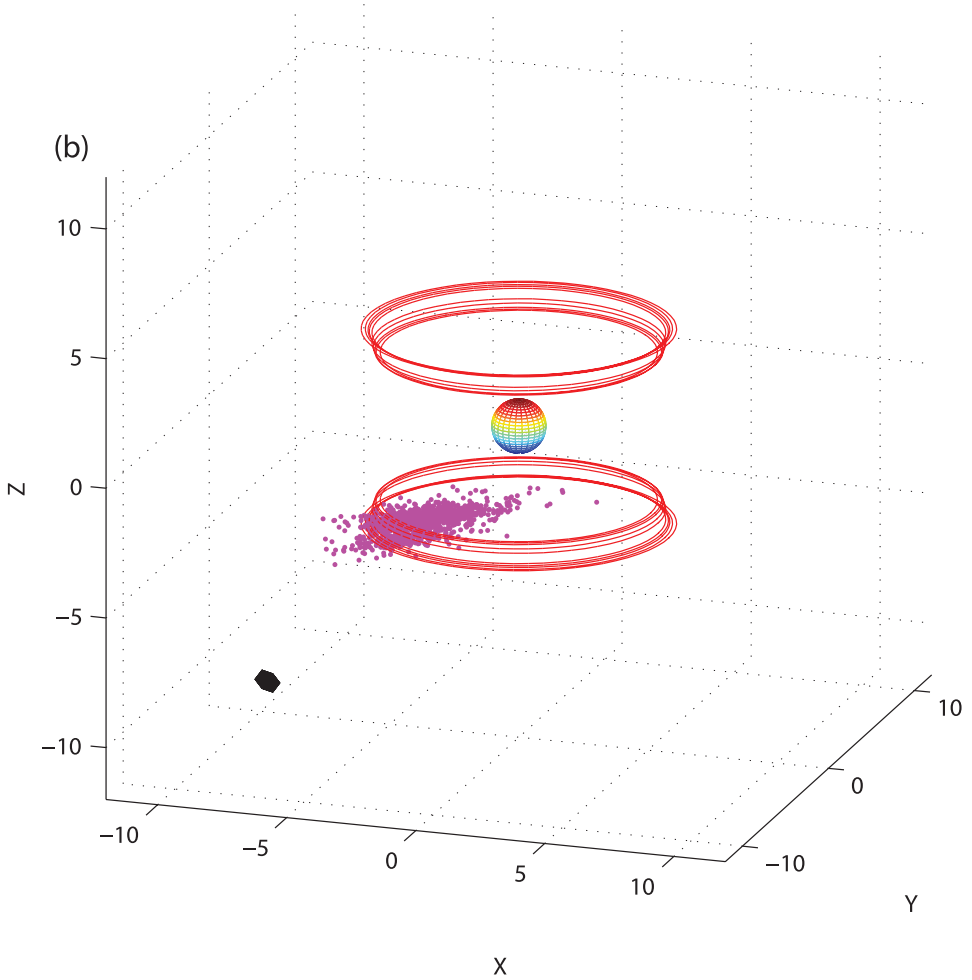

Figure 6. (a) Dynamic spectrogram and (bottom) 3-D source location of the 5-kHz narrowband emission observed by Cassini/RPWS from 2200 to 2300 SCET of DOY 363, 2006. Note that the source is in the southern hemisphere.

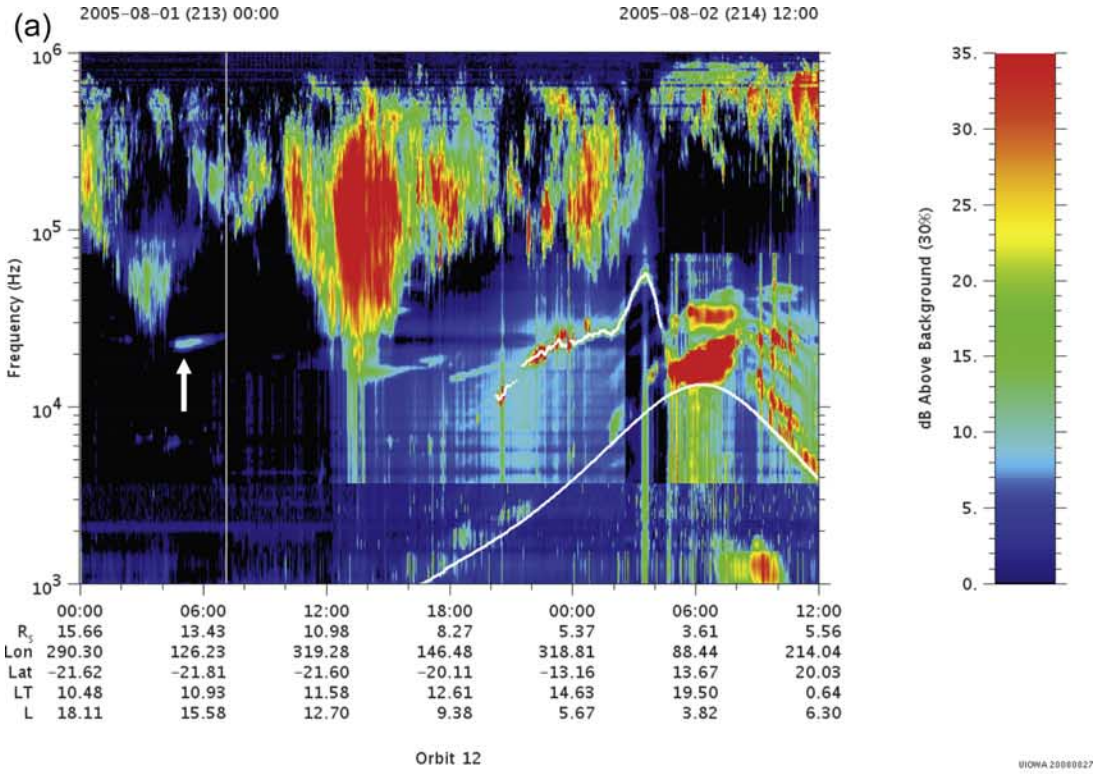

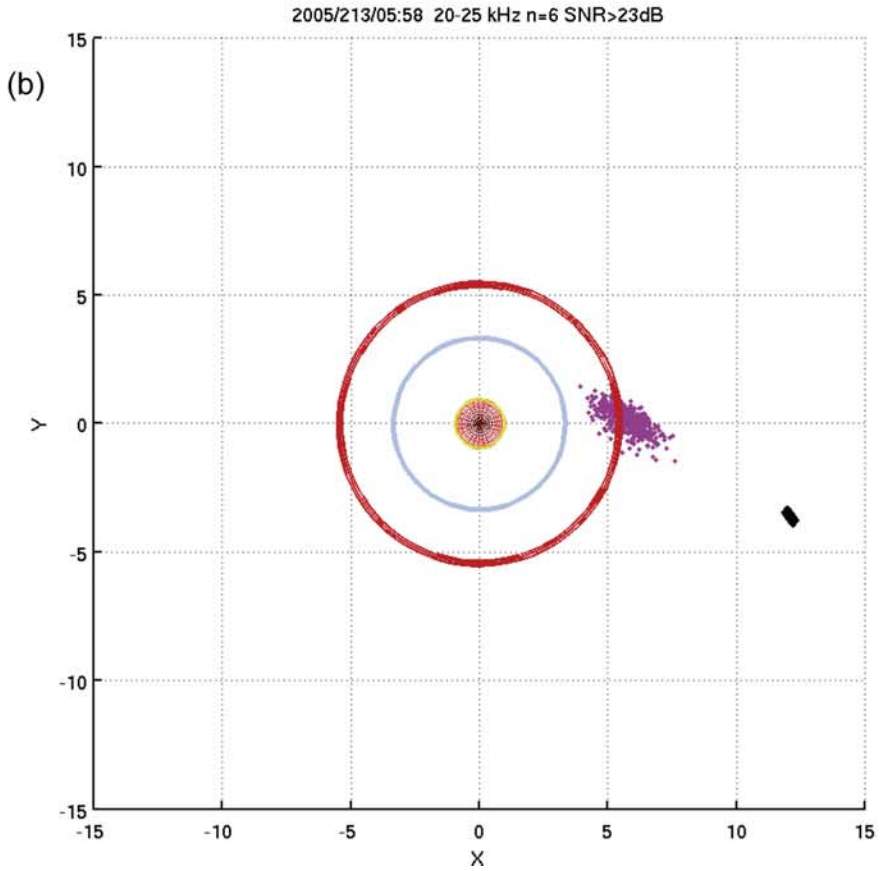

Figure 7. (a) Dynamic spectrogram and (b) a top view of the 3-D source location of the 20-kHz narrowband emission observed by Cassini/RPWS from 05 to 06 SCET of DOY 213, 2005. Cassini was at $\sim -22^{\circ}$ latitude and $\sim 14R_S$ away from Saturn. The HFR was operating in the dipole-monopole mode. The red and faint blue source rings in Figure 7b represent the modeled southern hemisphere source locations of the 20-kHz narrowband emissions, with harmonic number $n = 6$ and 1, respectively.

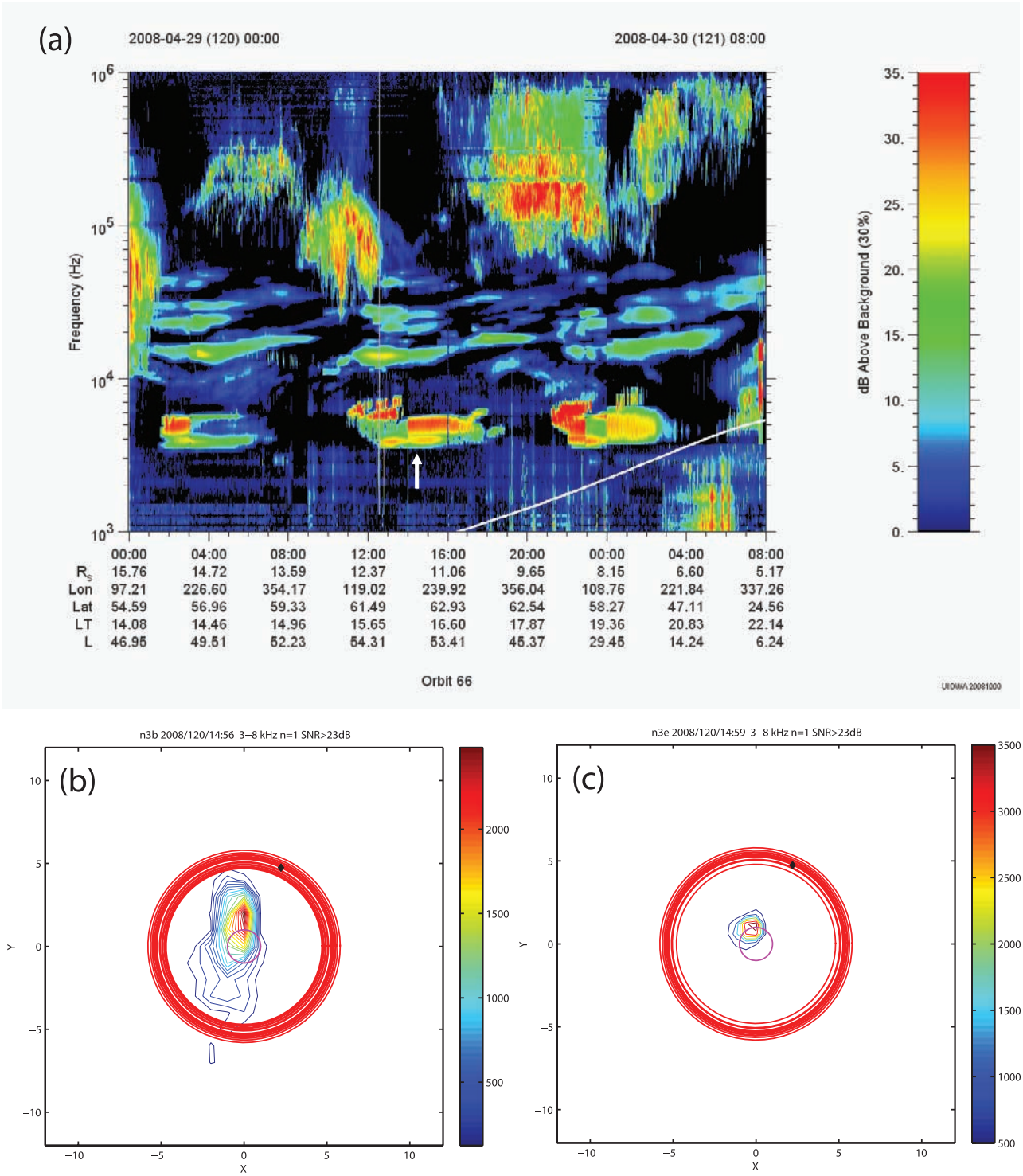

Figure 8. Comparison between the modeled source location of a narrowband emission and both the two-antenna and the three-antenna goniopolarimetric results. (a) Cassini RPWS spectrogram showing narrowband emissions observed on DOY 120, 2008. (b) The three-antenna goniopolarimetric results from 1400 to 1500 SCET (marked with an arrow in Figure 8a). (c) Results of two-antenna goniopolarimetric inversion applied to the three-antenna mode data of the same time interval.

direction of arrival (**E** plane normal) is not the direction of the **k** vector; (2) the point source assumption might not be valid, for example, multiple sources or an extended source, in which case the goniopolarimetry determines the centroid of the source; and (3) if the directions of arrival are correct, then these 5-kHz narrowband emissions are probably generated in some way other than mode conversion of ESUH waves on the edges of the plasma torus.

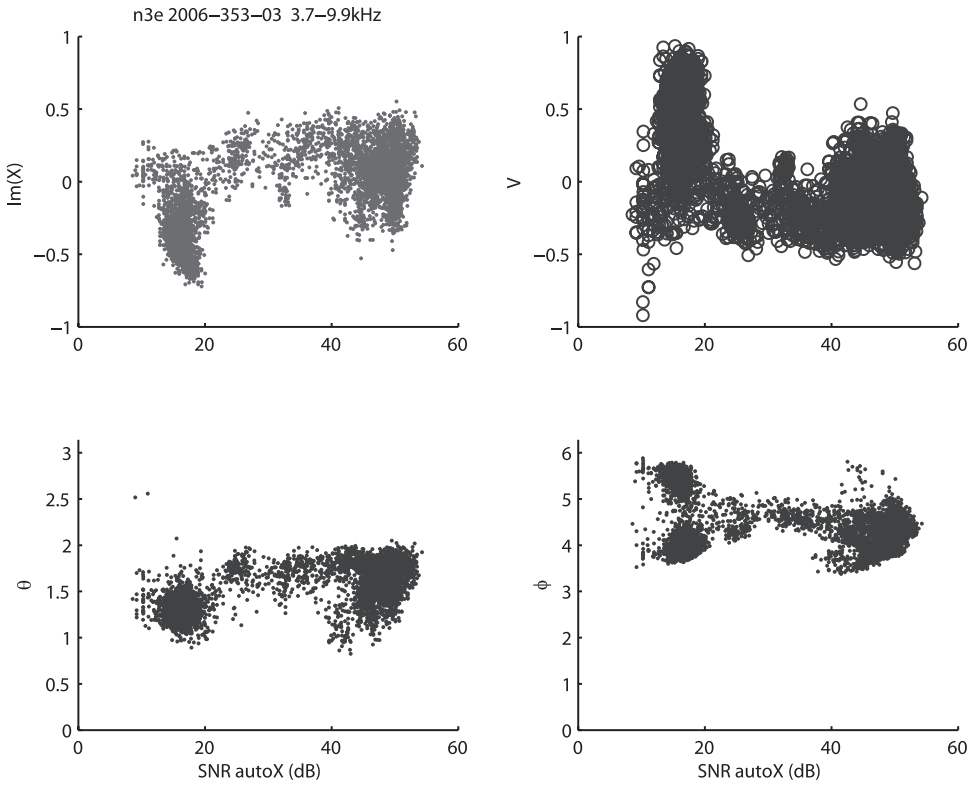

Figure 9. The two-antenna goniopolarimetric results for a very intense narrowband emission (>50 dB) observed from 03 to 04 SCET of DOY 353, 2006. The circular polarization degree of this narrowband emission does not approach either 1 or −1, whereas $U = 0$, $Q = 0$ have been assumed in the goniopolarimetric inversion. This indicates that the waves are partially polarized, which is confirmed by the emission's low apparent total polarization. The values of θ and ϕ are not well converged.

6.4. Discussion on the Comparison Between the Model and Goniopolarimetric Results

[38] Most of the case studies presented above show a good agreement between the goniopolarimetric results and the modeled source locations of the narrowband emissions, except for the last example, when the spacecraft is relatively close to Saturn. The events shown are selected on the basis of two criteria: (1) high intensity and (2) high degree of polarization. Criterion 1 is achieved by setting a threshold of the signal-to-noise ratio at 23 dB, which eliminates the data points that could be affected by the background subtraction.

[39] Criterion 2 turns out to be very important too. For those partially polarized or unpolarized narrowband emissions, the goniopolarimetric results show a lot of scatter even with high intensity levels, and it is difficult to compare them with the model. As an example, the two-antenna goniopolarimetric result of a partially polarized narrowband emission is shown in Figure 9. It can be seen that a partially polarized narrowband radio emission shows a significant scatter in the imaginary part of the cross correlation, which is not the case for a completely polarized wave as displayed in Figure 4. The reason why the 5 kHz narrowband emissions sometimes are partially or not polarized is not well understood, yet. In contrast to the 5-kHz narrowband emissions, the 20-kHz narrowband emissions are nearly always highly polarized, even though the intensity level is much lower than that of the 5-kHz emissions. As a result, the directions of arrival for the 20-kHz emissions are generally better defined and match the model better. This difference between the 5-kHz and 20-kHz narrowband emissions could be due to a quieter and less variable background level at higher frequencies and due to refraction effects.

[40] The goniopolarimetric results also revealed that the sources of narrowband emissions do not corotate with the planet, which supports the argument of Wang et al. (submitted manuscript, 2008) that the modulation of the 5-kHz narrowband emission is more like a clock than a rotating beam. It is also shown that sometimes the source of narrowband emissions are not restricted to the meridian plane of Cassini, which conflicts with the theory of *Jones* [1980], which says the emission should be confined to the plane containing the magnetic field and the density gradient. Further, the fact that narrowband emission can be observed at nearly all latitudes seems to indicate that the radio emission is not tightly beamed either.

7. Direction Finding Using Apparent Polarization Reversal

[41] In order to further verify the results of the two-antenna and three-antenna goniopolarimetry, we have also employed a polarization reversal technique to determine the source location of narrowband radio emission.

[42] As we stated, in the two-antenna goniopolarimetric inversion, there are 6 unknowns (S, Q, U, V, θ and ϕ) to

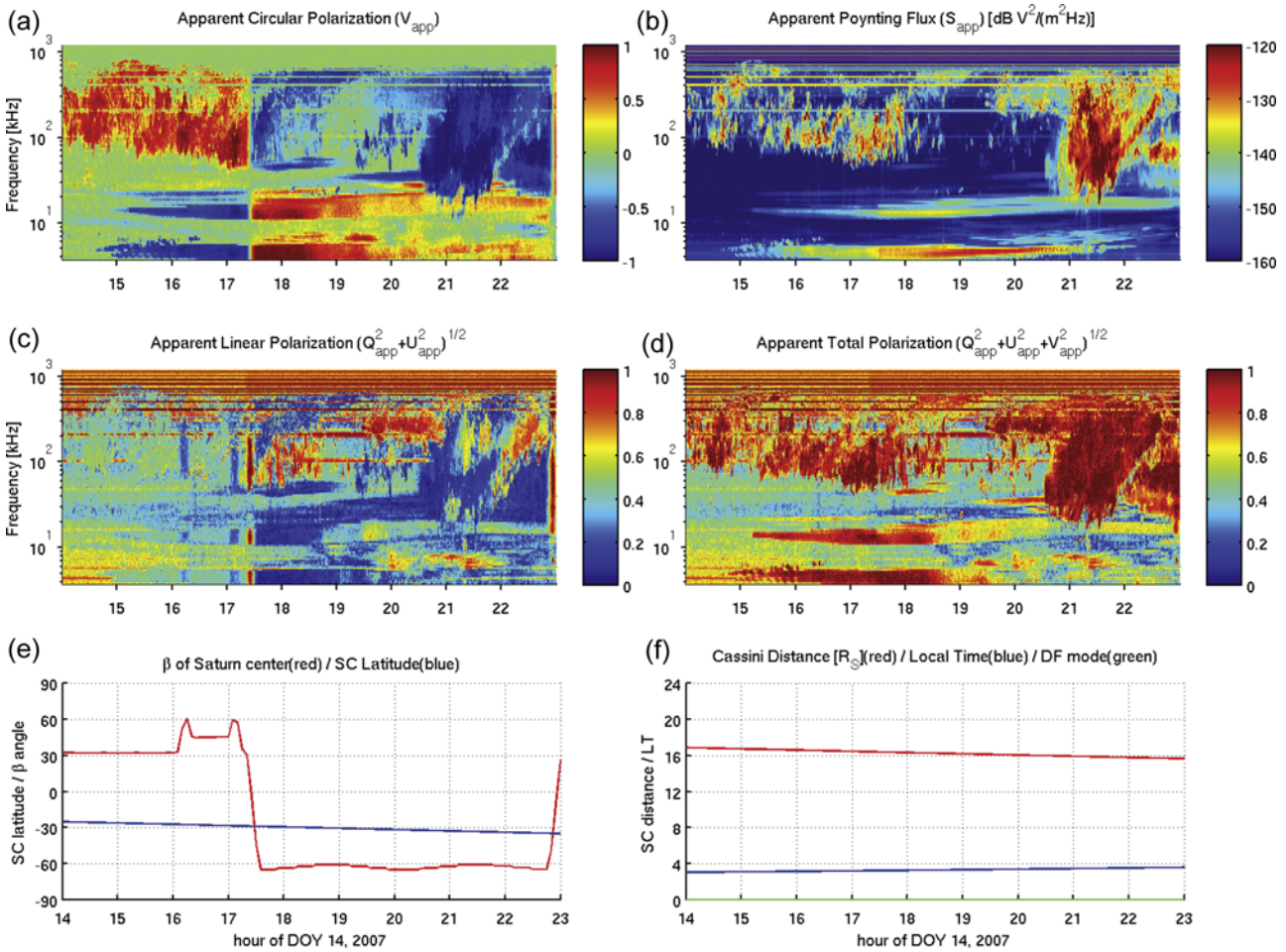

Figure 10. The apparent polarizations ((a) V_{app}, (b) S_{app}, (c) $\sqrt{Q_{app}^2 + U_{app}^2}$, and (d) $\sqrt{Q_{app}^2 + U_{app}^2 + V_{app}^2}$) calculated from RPWS/HFR data of DOY 014, 2007, and (e) and (f) the geometry of Cassini.

solve for in the equations on the basis of only 4 measurements. So assumptions need to be made for 2 of the 6 unknowns in order to solve the equations. For example, to calculate the Stokes parameters (S, Q, U, V) of a radio wave, assumptions on the direction of arrival are needed. When Cassini is far away from Saturn, the direction of arrival can be approximated to be the direction to the center of Saturn. However, this assumption is not valid when the spacecraft is close to the planet. Nonetheless, it is possible to characterize the polarization of the radio waves without prior knowledge of their directions of arrival, using the so-called apparent polarization. Formulas for calculating the apparent polarization of radio waves measured by two RPWS antennas have been derived by G. Fischer et al. (Elliptical polarization of Saturn kilometric radiation observed from high latitudes, submitted to *Journal of Geophysical Research*, 2009). The apparent Stokes parameters can be expressed in terms of the antenna measurement values as:

$$S_{app} = \frac{\langle V_x V_x^* \rangle}{h_x^2} + \frac{\langle V_w V_w^* \rangle}{h_w^2} \tag{1}$$

$$S_{app} q_{app} = \frac{\langle V_x V_x^* \rangle}{h_x^2} - \frac{\langle V_w V_w^* \rangle}{h_w^2} \tag{2}$$

$$S_{app} u_{app} = \frac{2Re\langle V_x V_w^* \rangle}{h_x h_w} \tag{3}$$

$$S_{app} v_{app} = \frac{2Im\langle V_x V_w^* \rangle}{h_x h_w} \tag{4}$$

where V_x and V_w are the voltage measurements on the E_x and and E_w antennas of Cassini RPWS, and h_x and h_w are the effective lengths of the two antennas. The asterisk * denotes the complex conjugate, and the brackets $\langle \cdots \rangle$ represent the averaging operation over the integration time.

[43] The apparent circular polarization switches sign when the source crosses through the antenna plane (the plane containing the effective axes of the two antennas) as the spacecraft is rotating [e.g., *Lecacheux and Ortega-*

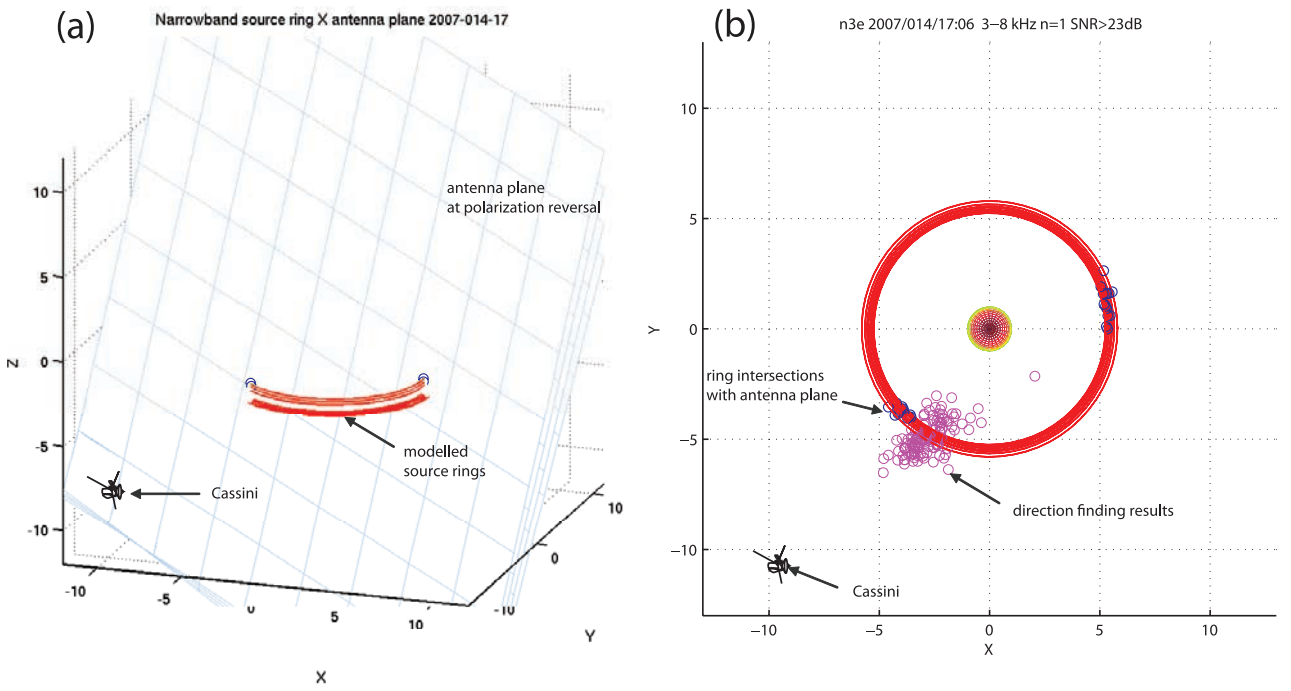

Figure 11. The 3-D source location of narrowband emissions using apparent circular polarization (V_{app}) reversal. (a) The intersection of the modeled source ring with the antenna plane when the measured V_{app} switches sign. (b) A comparison between the result of polarization reversal and the result of goniopolarimetry.

Molina, 1987]. Thus the source location of narrowband emissions can be determined by finding the intersection of the antenna plane with the modeled source ring at the moment of apparent polarization reversal.

[44] Figure 10 shows the apparent polarization calculated from the HFR data from DOY 14, 2007. Such plots have been created for every day since DOY 001, 2004. Shown are the spectrograms for (a) the apparent circular polarization degree V_{app}, (b) the apparent Poynting flux S_{app} in dB $V^2/(m^2Hz)$, (c) the apparent linear polarization degree, and (d) the apparent total polarization degree. The horizontal axes give the spacecraft event time (SCET). The vertical axes show the logarithmically scaled frequency in kHz. The color bar of apparent circular polarization ranges from −1 (blue) for apparent right-hand polarization to +1 (red) for apparent left-hand polarization.

[45] Narrowband emissions can be seen at 5 kHz from about 1500 to 2200 SCET and at 20 kHz from 1530 to 2300 SCET. The intense impulsive emissions above 20 kHz are SKR, which also extends slightly below 20 kHz from about 2030 to 2130 SCET. The spacecraft was about 16 R_S from Saturn, around −30° latitude. At about 1725 SCET, the apparent circular polarization degree of both SKR and narrowband emissions are reversed, indicating that the source of both radio emissions goes from one side of the antenna plane to the other because of the rotation of Cassini. At this instant, the apparent linear polarization degree of both SKR and narrowband emissions are equal to 1, which is expected because the phase difference between the signals on the two antennas is zero when the source is in the antenna plane.

[46] The position and attitude of Cassini are also shown in Figures 10e and 10f. Figure 10e shows the latitude (blue curve) of the spacecraft and the β angle (red curve) between the antenna plane (the one containing the effective axes of dipole E_x and monopole E_w antenna) and the direction to the center of Saturn. Figure 10f shows the radial distance (red curve) and local time (blue curve) of the spacecraft. The direction-finding mode status of the HFR is also shown in Figure 10f with the green curve, where 0 means the receiver operates in dipole-monopole mode (two-antenna mode) and 1 means the receiver operates in direction-finding mode (three-antenna mode).

[47] Figure 11a shows the source location of the narrowband emission using the polarization reversal technique. The antenna plane of the spacecraft when V_{app} switches sign is plotted together with the modeled source locations for the 5 kHz narrowband emission at the southern edge of the plasma disk, the red rings. The intersection points between the antenna plane and the source rings, marked with blue circles, indicate possible source locations of the narrowband emission. Figure 11b compares the two source localization methods. The source locations obtained from the polarization reversal method, blue circles, are plotted on top of the two-antenna goniopolarimetric results, drawn as magenta circles. These results from the two methods are reasonably consistent. A number of factors could have contributed to the small observed difference. For example, the inaccuracy of the direction of arrivals, which could be greater than 2° when the source is close to the antenna plane [*Cecconi and Zarka*, 2005]. The inaccuracy in the location of the modeled source ring based on the model uncertainty would also significantly affect the locations of the intersection points. The model uncertainty includes uncertainty in the empirical density model of the plasma torus, uncertainty in the

magnetic field model, and uncertainty in the matching condition; that is, the 1/2 in $(n + 1/2)f_{ce}$ could be anything between 0 and 1. The refraction effects cannot explain the discrepancy since it presumably affects both types of measurement identically.

8. Discussion

[48] Counterparts of Saturn narrowband radio emissions (otherwise called n-SMR or n-SKR) are detected at the Earth, Jupiter, Uranus, Neptune and even the Jovian moon Ganymede [*Kurth et al.*, 1997]. Although there has been a long series of experimental and theoretical works trying to determine the source location, beaming pattern, polarization and generation mechanism of narrowband emission, it remains controversial how this type of emission is generated and how it is related to plasmaspheric dynamics. The proposed generation mechanisms can be roughly categorized as (1) linear mode conversion [*Jones*, 1976; *Budden and Jones*, 1987; *Horne*, 1989], (2) nonlinear mode conversion (wave-wave interaction) [*Melrose*, 1981; *Barbosa*, 1982; *Rönnmark*, 1983; *Murtaza and Shukla*, 1984; *Rönnmark*, 1985], (3) radiation from collapsing upper hybrid solitons [*Christiansen et al.*, 1984], and (4) direct generation via relativistic cyclotron harmonic maser [*Farrell*, 2001; *Farrell et al.*, 2004]. Most of the studies assume that the narrowband emission is generated in two steps: first, an intense electrostatic wave is generated when the matching condition $f_{UH} = (n + 1/2)f_{ce}$ is satisfied; and then the electrostatic wave is converted to an escaping electromagnetic wave via either a linear or a nonlinear mode conversion process.

[49] The mode conversion generation mechanism has also been applied to auroral roar, a terrestrial auroral radio emission generated at the top and bottom sides of the auroral ionosphere when $f_{UH} \cong 2$ or $3f_{ce}$ [*Yoon et al.*, 1996, 1998; *LaBelle and Treumann*, 2002]. It is interesting that nonthermal continuum and auroral roar are found to have similar fine structures (striations). The fine structure of auroral roar is explained by eigenmode trapping of Z mode emissions within field aligned density enhancements [*Yoon et al.*, 2000, 2007; *Ye et al.*, 2007]. This eigenmode trapping theory has been modified to explain the fine structures in planetary continuum radiations [*Yoon and Menietti*, 2005; *Menietti and Yoon*, 2006; *Menietti et al.*, 2007].

[50] In this study, the source location model is based on the assumption that the narrowband emissions are generated by mode conversion from ESUH waves on the edges of the plasma torus. The validity of this assumption is supported by multiple source crossing events for the 20-kHz narrowband emissions, although no such source crossing has been observed for the 5-kHz emission. The source locations derived from both goniopolarimetric results and the polarization reversal method seem to be consistent with the model, at least for the 20-kHz emission, which also lends support to the mode conversion theory. For the 5-kHz narrowband emissions, some goniopolarimetric results are consistent with the model predictions while some results seem to indicate higher-latitude sources, especially when Cassini is close to Saturn. In these higher-latitude regions, f_{pe} is much lower than f_{ce} and no ESUH waves has been observed, thus the mode conversion mechanism could not apply to these 5-kHz narrowband emissions. It is also possible that the narrowband emissions are generated on the inner edge of the plasma torus. However, the measured polarization, in this case, would not be consistent with a L-O mode emission, because the left-handed polarization observed from the northern hemisphere would have beaming angles exceeding 90° for sources close to the equatorial plane. It would also be difficult for the narrowband emissions generated here to be observed by Cassini on a low-latitude orbit outside the plasma torus.

[51] Although Saturn narrowband emissions have been detected in the frequency range from 3 to 70 kHz (e.g., Figure 12), their occurrence probability and wave intensity are higher around 5 and 20 kHz. What favors the generation or propagation of narrowband emissions at these two frequencies still remains a mystery. In both linear and nonlinear mode conversion theories, the existence of sharp density gradients is a required condition for the electrostatic waves to be converted to electromagnetic emissions. It might be the case that the electrostatic waves are excited at all frequencies around the predicted source locations for them, but sharp density gradients preferentially exist around the source location of the 5-kHz and the 20-kHz narrowband emissions. It is also possible that the 5-kHz and the 20-kHz narrowband emissions have different source mechanisms, given their differences in time-frequency structures and the fact that no source crossing for the 5-kHz narrowband emissions has been observed so far.

[52] Examination of the apparent polarization plots for the time interval between 2004 and 2008 show that most narrowband emissions are propagating in the L-O mode, with some exceptions at frequencies > 20 kHz. These exceptions are determined to be R-X mode emissions generated at second harmonic frequencies of the fundamental L-O mode emissions. Such emissions suggest a nonlinear mode conversion process. Figure 13 shows the apparent polarizations of RPWS data that covers 30 h starting from 1000 SCET of DOY 129, 2007. In Figure 13a, which shows the apparent Poynting flux, four pairs of fundamental and harmonic narrowband emissions are centered around 1200, 2000 SCET (DOY 129), 0600 and 1400 SCET (DOY 130). The intensities of the fundamental and harmonic emissions are observed to vary coherently. In Figure 13b, the apparent circular polarization of the harmonic emission is identical to that of the SKR and opposite to that of the fundamental narrowband emission. At the fourth pair, the sense of polarization is reversed (for narrowband emissions as well as SKR) because of a change in spacecraft attitude. Goniopolarimetric results also show that the fundamental and harmonic emissions have nearly identical directions of arrival, ruling out the possibility that beaming angle crossing 90° may have caused the polarization change. Therefore, the harmonic narrowband emissions should be emitted in R-X mode.

[53] *James et al.* [1974] show observations by ISIS satellites of strong narrowband emissions around 2 and 4 MHz at auroral latitudes, believed to be emitted from the top side of the Earth's ionosphere. They propose that the 2 MHz emissions are O mode waves generated where $f_{UH} = 2f_{ce}$ by mode coupling with Bersntein waves. On the basis of ray tracing, the source altitude of the higher-frequency band is determined to be within the experimental error of the lower-frequency band source altitude. The

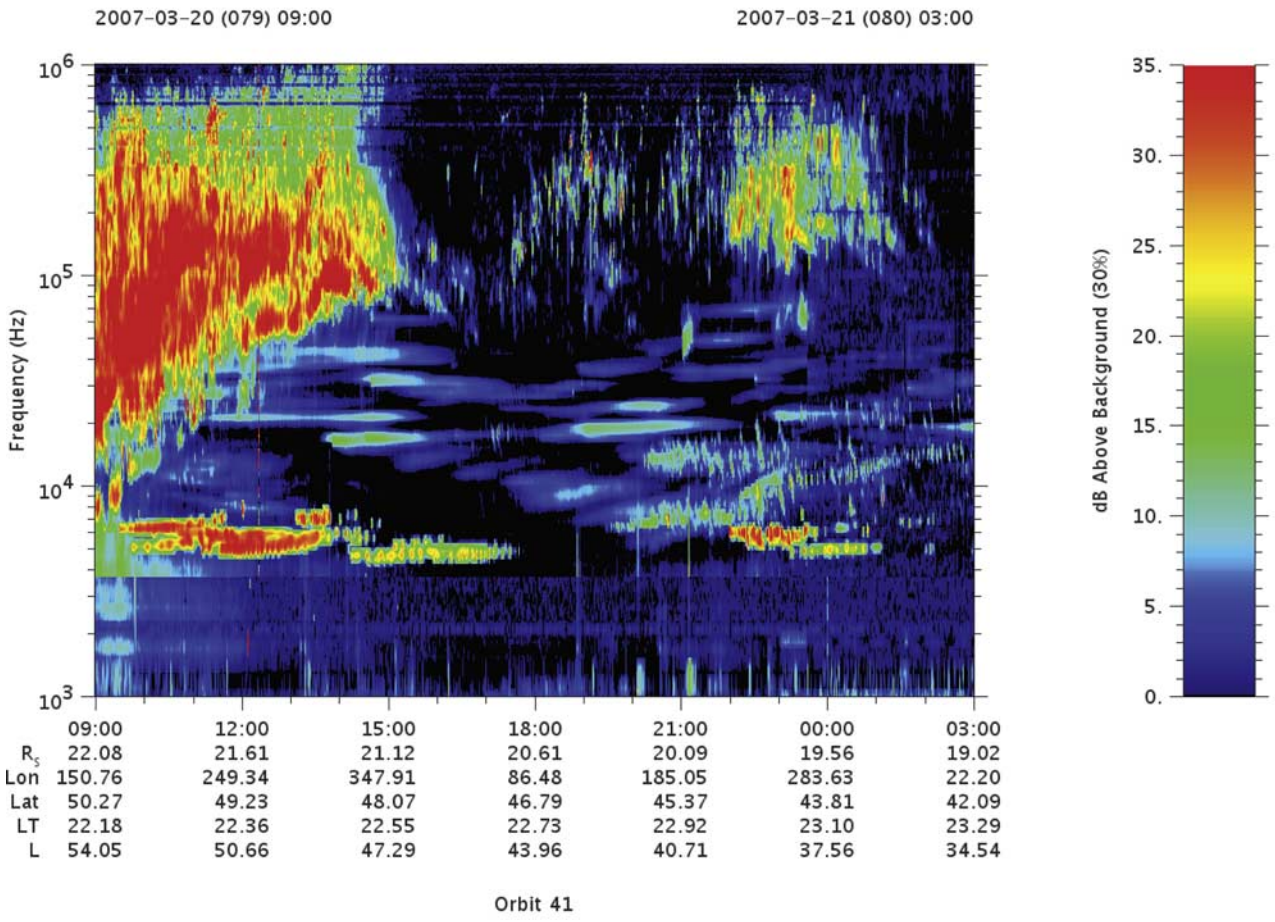

Figure 12. A Cassini RPWS spectrogram showing detection of Saturn narrowband emissions with frequencies up to 70 kHz.

common source location and the higher band being at the second harmonic frequency of the lower band point to wave-wave interactions for the generation of the harmonic emissions at 4 MHz. *Roux and Pellat* [1979] discuss a coherent nonlinear three-wave process to generate R-X mode emission at $2f_{UH}$. *Melrose* [1991] proposes that the harmonic structures in solar radio bursts are the result of coalescence of Z mode waves. *Willes et al.* [1998] use the same coalescence theory to explain the generation of auroral roar emissions at harmonics of electron cyclotron frequency. If nonlinear mode conversion applies to narrowband emissions, then the L-O mode fundamental could be generated by the wave-wave interaction between the electrostatic wave at f_{UH} and electrostatic waves at lower hybrid frequencies [*Melrose*, 1981; *Barbosa*, 1982], and the R-X mode second harmonic could be generated by a wave-wave interaction between two electrostatic waves at the upper hybrid frequency with opposite **k** vectors.

9. Summary and Future Work

[54] A model for the narrowband emission source location is constructed on the basis of the electron density profile of Saturn's plasma torus given by *Persoon et al.* [2006] and a dipole magnetic field model [*Ness et al.*, 1981]. The source locations of narrowband emissions were determined by calculating the locations where the matching condition, $f_{UH} = (n + 1/2)f_{ce}$, is met. For narrowband emissions of a certain frequency, multiple source locations corresponding to different harmonic numbers ($n = 1, 2, 3, \cdots$) are predicted by the model. Although required by mode conversion theories [*Jones*, 1976; *Melrose*, 1981], the existence of a density gradient is not considered in this model. Because of the relatively weak magnetic field of Saturn, the modeled source locations of narrowband radio emissions ($n < 3$) lie on the northern and southern edges of the plasma torus as opposed to the outer edge of the Io plasma torus in the case of Jovian n-KOM. These locations could actually explain why 20-kHz narrowband emissions are less frequently observed in the equatorial plane when Cassini is far away from the planet, because the radio waves would be refracted by the plasma torus to higher latitudes.

[55] In several cases when Cassini passes through the source region of the 20-kHz narrowband emissions, the positions of the spacecraft are shown to agree with the source locations predicted by the model. No convincing source crossing of the 5-kHz narrowband emissions has been observed. However, because of orbit limitations, there were very few opportunities for Cassini to pass through the model predicted source region of the 5-kHz narrowband emissions. The two-antenna goniopolarimetric results of Cassini RPWS confirm that the model is a good predictor for the source

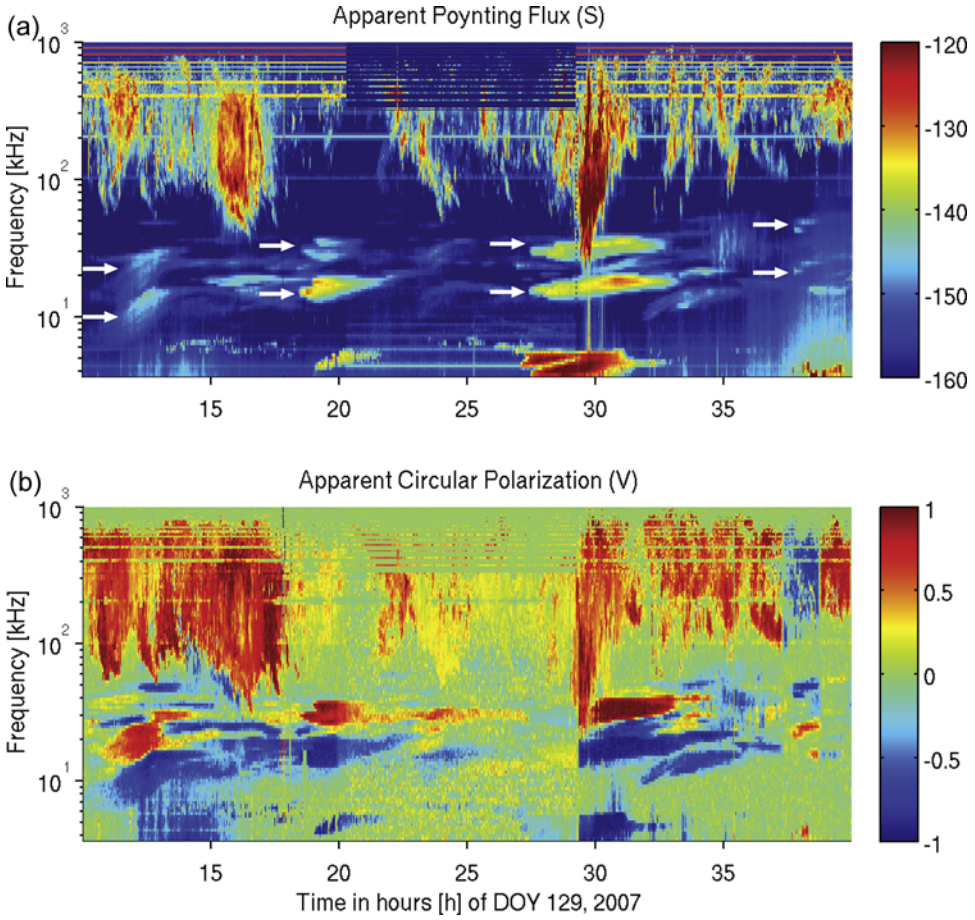

Figure 13. Narrowband emissions with oppositely polarized harmonics detected by Cassini/RPWS on DOY 129 and on DOY 130, 2007. (a) The apparent Poynting flux S_{app} and (b) the apparent circular polarization v_{app}.

location of narrowband emissions, although, since we do not know the local parameters at the source, assumptions on the *n* number are needed. The two-antenna goniopolarimetric inversion is applied to the three-antenna mode data, and the result is consistent with the three-antenna goniopolarimetric result which does not rely on any assumption of the wave polarization parameters. A polarization reversal technique was applied to determine the source location of circularly polarized radio emissions, such as narrowband emission. The polarization reversal technique is very accurate and gave results comparable to the goniopolarimetric measurement of RPWS.

[56] The prediction by mode conversion theories [*Jones*, 1976; *Melrose*, 1981] that the nonthermal continuum radiation are emitted in the L-O mode is confirmed. Most of the narrowband emissions are determined to be in the L-O mode. However, some narrowband radio emissions above 20 kHz are also found to be oppositely polarized to the other narrowband emissions, which could be caused by a special observation geometry or a different generation mechanism. Some evidence has been found to support a nonlinear mode conversion (wave-wave interaction) mechanism for the generation of the >20 kHz R-X mode narrowband harmonic emissions. Additionally, goniopolarimetric results contradict the predictions of linear mode conversion theory, for example, the restriction of the emissions to the meridian plane. The wide range of latitudes that the narrowband emissions can be observed over also opposes the latitudinal beaming prediction of the linear mode conversion theory [*Jones*, 1980]. This is consistent with the results of *Morgan and Gurnett* [1991], *Hashimoto et al.* [2005], and *Boardsen et al.* [2008], who did not observe the latitudinal beaming effect of continuum radiation reported by *Jones* [1987].

[57] The relationship between the occurrence of narrowband emissions and Saturn's plasmaspheric dynamics is still not well understood. Wang et al. (submitted manuscript, 2008) argue that the narrowband emissions are related to the energetic plasma injection during a period of high magnetic activity, which is indicated by intensification of SKR. Energetic neutral atoms (ENA) observations by the MIMI/INCA experiment onboard Cassini reveals the activity of the high-energy ions in Saturn's magnetosphere. *Carbary et al.* [2008] show that the radial distribution of the ENA emission centroids maximizes near the orbit of Rhea ($\sim 9\ R_S$), which also agrees with the source location of narrowband emissions predicted by the model built in this paper. A case by case comparison between the ENA images and the RPWS goniopolarimetric results is needed to confirm the relationship between the narrowband emissions and the injected hot plasma. So far, the goniopolarimetric results show that the sources of the 20-kHz and the-5 kHz narrowband emissions stay almost fixed in local time and are not

restricted within the meridian plane of the spacecraft. These results seem to be consistent with the clock like modulation of narrowband emissions discovered by Wang et al. (submitted manuscript, 2008). The reason why Kronian narrowband emissions do not act like a rotating beam as Jovian n-KOM but more like a clock remains a mystery.

[58] **Acknowledgments.** The research reported in this paper was supported by NASA and the Cassini project through contract 1279973 from the Jet Propulsion Laboratory. The first author thanks Ann Persoon for the help on illustrations.

[59] Amitava Bhattacharjee thanks James LaBelle and Robert Benson for their assistance in evaluating 2008JA013855.

References

Ashour-Abdalla, M., and C. F. Kennel (1978), Non-convective and convective electron-cyclotron harmonic instabilities, *J. Geophys. Res.*, *83*, 1531.

Barbosa, D. D. (1982), Low-level VLF and LF radio emissions observed at Earth and Jupiter, *Rev. Geophys.*, *20*, 316.

Benson, R., V. Osherovich, J. Fainberg, A. F. Vinas, and D. Ruppert (2001), An interpretation of banded magnetospheric radio emissions, *J. Geophys. Res.*, *106*, 13,179.

Boardsen, S. A., J. L. Green, and B. W. Reinisch (2008), Comparison of kilometric continuum latitudinal radiation patterns with linear mode conversion theory, *J. Geophys. Res.*, *113*, A01219, doi:10.1029/2007JA012319.

Budden, K. G., and D. Jones (1987), Conversion of electrostatic upper hybrid emissions to electromagnetic O-mode and X-mode waves in the Earth's magnetosphere, *Ann. Geophys.*, *5*, 21.

Carbary, J. F., D. G. Mitchell, P. Brandt, E. C. Roelof, and S. M. Krimigis (2008), Track analysis of energetic neutral atom blobs at Saturn, *J. Geophys. Res.*, *113*, A01209, doi:10.1029/2007JA012708.

Cecconi, B. (2007), Influence of an extended source on goniopolarimetry (or direction finding) with Cassini and Solar Terrestrial Relations Observatory radio receivers, *Radio Sci.*, *42*, RS2003, doi:10.1029/2006RS003458.

Cecconi, B., and P. Zarka (2005), Direction finding and antenna calibration through analytical inversion of radio measurements performed using a system of two or three electric dipole antennas on a three-axis stabilized spacecraft, *Radio Sci.*, *40*, RS3003, doi:10.1029/2004RS003070.

Cecconi, B., L. Lamy, P. Zarka, R. Prangé, W. S. Kurth, and P. Louarn (2009), Goniopolarimetric study of the Rev 29 perikrone using the Cassini/RPWS/HFR radio receiver, *J. Geophys. Res.*, *114*, A03215, doi:10.1029/2008JA013830.

Christiansen, P. J., J. Etcheto, K. Rönnmark, and L. Stenflo (1984), Upper hybrid turbulence as a source of nonthermal continuum radiation, *Geophys. Res. Lett.*, *11*, 139.

Farrell, W. M. (2001), Direct generation of O-mode emission in a dense, warm plasma: Applications to interplanetary type II emissions and others in its class, *J. Geophys. Res.*, *106*, 15,701.

Farrell, W. M., M. L. Kaiser, W. S. Kurth, M. D. Desch, D. A. Gurnett, G. B. Hospodarsky, and R. J. MacDowall (2004), Remote sensing of possible plasma density bubbles in the inner Jovian dayside magnetosphere, *J. Geophys. Res.*, *109*, A09S14, doi:10.1029/2003JA010130.

Farrell, W. M., W. S. Kurth, M. L. Kaiser, M. D. Desch, D. A. Gurnett, and P. Canu (2005), Narrowband Z-mode emissions interior to Saturn's plasma torus, *J. Geophys. Res.*, *110*, A10204, doi:10.1029/2005JA011102.

Frankel, M. S. (1973), LF radio noise from the Earth's magnetosphere, *Radio Sci.*, *8*, 991.

Fung, S., and K. Papadopoulos (1987), The emission of narrow-band Jovian kilometric radiation, *J. Geophys. Res.*, *92*, 8579.

Gurnett, D. A., and R. R. Shaw (1973), Electromagnetic radiation trapped in the magnetosphere above the plasma frequency, *J. Geophys. Res.*, *78*, 8136.

Gurnett, D. A. (1974), The Earth as a radio source: Terrestrial kilometric radiation, *J. Geophys. Res.*, *79*, 4227.

Gurnett, D. A. (1975), The Earth as a radio source - nonthermal continuum, *J. Geophys. Res.*, *80*, 2751.

Gurnett, D. A., and A. Bhattacharjee (2005), *Introduction to Plasma Physics With Space and Laboratory Applications*, pp. 124–125, Cambridge Univ. Press, Cambridge, U. K.

Gurnett, D. A., W. S. Kurth, and F. L. Scarf (1981), Narrowband electromagnetic emissions from Saturn's magnetosphere, *Nature*, *292*, 733.

Gurnett, D. A., W. Calvert, R. Huff, D. Jones, and M. Sugiura (1988), The polarization of escaping terrestrial continuum radiation, *J. Geophys. Res.*, *93*, 12,817.

Gurnett, D. A., et al. (2004), The Cassini radio and plasma wave investigation, *Space Sci. Rev.*, *114*, 395.

Gurnett, D. A., et al. (2005), Radio and plasma wave observations at Saturn from Cassini's approach and first orbit, *Science*, *307*, 1255, doi:10.1126/science.1105356.

Hashimoto, K., R. R. Anderson, J. L. Green, and H. Matsumoto (2005), Source and propagation characteristics of kilometric continuum observed with multiple satellites, *J. Geophys. Res.*, *110*, A09229, doi:10.1029/2004JA010729.

Horne, R. B. (1989), Path-integrated growth of electrostatic waves: The generation of terrestrial myriametric radiation, *J. Geophys. Res.*, *94*, 8895.

Hubbard, R., and T. Birmingham (1978), Electrostatic emissions between electron gyroharmonics in the outer magnetosphere, *J. Geophys. Res.*, *83*, 4837.

James, H. G., E. L. Hagg, and D. L. P. Strange (1974), Narrowband radio noise in the topside ionosphere, *AGARD Conf. Proc., AGARD-CP-138,* 24-1.

Jones, D. (1976), Source of terrestrial nonthermal radiation, *Nature*, *260*, 686.

Jones, D. (1980), Latitudinal beaming of planetary radio emissions, *Nature*, *288*, 225.

Jones, D. (1987), Observed beaming of terrestrial myriametric radiation, *Nature*, *328*, 391.

Jones, D. (1988), Planetary radio emissions from low magnetic latitudes: Observations and theories, in *Planetary Radio Emissions II*, edited by H. O. Rucker, S. J. Bauer, and M. L. Kaiser, pp. 255–293, Austrian Acad. of Sci. Press, Vienna.

Krimigis, S. M., et al. (2004), Magnetosphere imaging instrument (MIMI) on the Cassini mission to Saturn/Titan, *Space Sci. Rev.*, *114*, 233.

Kurth, W. S. (1982), Detailed observations of the source of terrestrial narrowband electromagnetic radiation, *Geophys. Res. Lett.*, *9*, 1341.

Kurth, W. S. (1992), Continuum radiation in planetary Magnetospheres, in *Planetary Radio Emissions III*, edited by H. O. Rucker, S. J. Bauer, and M. L. Kaiser, pp. 329–350, Austrian Acad. of Sci. Press, Vienna.

Kurth, W. S., J. D. Craven, L. A. Frank, and D. A. Gurnett (1979a), Intense electrostatic waves near the upper hybrid resonance frequency, *J. Geophys. Res.*, *84*, 4145.

Kurth, W. S., M. Ashour-Abdalla, L. Frank, C. Kennel, D. A. Gurnett, D. Sentman, and B. Burek (1979b), A comparison of intense electrostatic waves near f_{UHR} with linear instability theory, *Geophys. Res. Lett.*, *6*, 487.

Kurth, W. S., D. A. Gurnett, and R. R. Anderson (1981), Escaping nonthermal continuum radiation, *J. Geophys. Res.*, *86*, 5519.

Kurth, W. S., D. A. Gurnett, A. Roux, and S. Bolton (1997), Ganymede: A new radio source, *Geophys. Res. Lett.*, *24*, 2167.

Labelle, J., and R. A. Treumann (2002), Auroral radio emissions, 1. Hisses, roars, and bursts, *Space Sci. Rev.*, *101*, 295.

LaBelle, J., D. Ruppert, and R. Treumann (1999), A statistical study of banded magnetospheric emissions, *J. Geophys. Res.*, *104*, 293.

Lamy, L., P. Zarka, B. Cecconi, R. Prangé, W. S. Kurth, and D. A. Gurnett (2008), Saturn kilometric radiation: Average and statistical properties, *J. Geophys. Res.*, *113*, A07201, doi:10.1029/2007JA012900.

Lecacheux, A., and A. Ortega-Molina (1987), Polarization and localization of the Uranian radio-sources, *J. Geophys. Res.*, *92*, 15,148.

Louarn, P., et al. (2007), Observation Of Similar Radio Signatures At Saturn And Jupiter: Implications For The Magnetospheric Dynamics, *Geophys. Res. Lett.*, *34*, L20113, doi:10.1029/2007GL030368.

Melrose, D. B. (1981), A theory for the nonthermal radio continua in the terrestrial and Jovian magnetospheres, *J. Geophys. Res.*, *86*, 30.

Melrose, D. B. (1991), Emission at cyclotron harmonics due to coalescence of Z-mode waves, *Astrophys. J.*, *380*, 256.

Menietti, J. D., and P. H. Yoon (2006), Plasma waves and fine structure emission bands within a plasmapause density cavity source region, *Geophys. Res. Lett.*, *33*, L15101, doi:10.1029/2005GL025610.

Menietti, J. D., R. R. Anderson, J. S. Pickett, D. A. Gurnett, and H. Matsumoto (2003), Near-source and remote observations of kilometric continuum radiation from multispacecraft observations, *J. Geophys. Res.*, *108*(A11), 1393, doi:10.1029/2003JA009826.

Menietti, J. D., O. Santolik, J. S. Pickett, and D. A. Gurnett (2005a), High resolution observations of continuum radiation, *Planet. Space. Sci.*, *53*, 283.

Menietti, J. D., D. A. Gurnett, and J. B. Groene (2005b), Radio emission observed by Galileo in the inner Jovian magnetosphere during orbit A-34, *Planet. Space. Sci.*, *53*, 1234.

Menietti, J. D., P. H. Yoon, and D. A. Gurnett (2007), Possible eigenmode trapping in density enhancements in Saturn's inner magnetosphere, *Geophys. Res. Lett.*, *34*, L04103, doi:10.1029/2006GL028647.

Morgan, D. D., and D. A. Gurnett (1991), The source location and beaming of terrestrial continuum radiation, *J. Geophys. Res.*, *96*, 9595.

Murtaza, G., and P. K. Shukla (1984), Nonlinear generation of electromagnetic waves in a magnetoplasma, *J. Plasma Phys.*, *31*, 423.

Ness, N. F., M. H. Acuna, R. P. Lepping, J. E. P. Connerney, K. W. Behannon, L. F. Burlaga, and F. M. Neubauer (1981), Magnetic-field studies by Voyager-1: Preliminary results at Saturn, *Science*, *212*, 211.

Persoon, A. M., D. A. Gurnett, W. S. Kurth, and J. B. Groene (2006), A simple scale height model of the electron density in Saturn's plasma disk, *Geophys. Res. Lett.*, *33*, L18106, doi:10.1029/2006GL027090.

Reiner, M., J. Fainberg, R. Stone, M. Kaiser, M. Desch, R. Manning, P. Zarka, and B.-M. Pedersen (1993), Source characteristics of Jovian narrow-band kilometric radio emissions, *J. Geophys. Res.*, *98*, 13,163.

Rönnmark, K. (1978), Banded electron cyclotron harmonic instability: A first comparison of theory and experiment, *Space Sci. Rev.*, *22*, 401.

Rönnmark, K. (1983), Emission of myriametric radiation by coalescence of upper hybrid waves with low-frequency waves, *Ann. Geophys.*, *1*, 187.

Rönnmark, K. (1985), Generation of magnetospheric radiation by decay of Bernstein waves, *Geophys. Res. Lett.*, *12*, 639.

Roux, A., and R. Pellat (1979), Coherent generation of the auroral kilometric radiation by non-linear beatings between electrostatic-waves, *J. Geophys. Res.*, *84*, 5189.

Scarf, F. L., D. A. Gurnett, W. S. Kurth, and R. L. Poynter (1982), Voyager-2 plasma-wave observations at Saturn, *Science*, *215*, 587.

Shaw, R., and D. A. Gurnett (1975), Electrostatic noise bands associated with the electron gyrofrequency and plasma frequency in the outer magnetosphere, *J. Geophys. Res.*, *80*, 4259.

Willes, A., S. Bale, and Z. Kuncic (1998), A *Z* mode electron-cyclotron maser model for bottomside ionospheric harmonic radio emissions, *J. Geophys. Res.*, *103*, 7017.

Wu, C. S., and L. C. Lee (1979), Theory of the terrestrial kilometric radiation, *Astrophys. J.*, *230*, 621.

Ye, S., J. LaBelle, P. H. Yoon, and A. T. Weatherwax (2007), Experimental tests of the eigenmode theory of auroral roar fine structure and its application to remote sensing, *J. Geophys. Res.*, *112*, A12304, doi:10.1029/2007JA012525.

Yoon, P. H., and J. D. Menietti (2005), On fine structure emission associated with plasmaspheric density irregularities, *Geophys. Res. Lett.*, *32*, L23103, doi:10.1029/2005GL023795.

Yoon, P., A. Weatherwax, T. Rosenberg, and J. LaBelle (1996), Lower ionospheric cyclotron maser theory: A possible source of $2f_{ce}$ and $3f_{ce}$ auroral radio emissions, *J. Geophys. Res.*, *101*, 27,015.

Yoon, P., A. Weatherwax, and T. Rosenberg (1998), On the generation of auroral radio emissions at harmonics of the lower ionospheric electron cyclotron frequency: *X*, *O* and *Z* mode maser calculations, *J. Geophys. Res.*, *103*, 4071.

Yoon, P., A. Weatherwax, and J. LaBelle (2000), Discrete electrostatic eigenmodes associated with ionospheric density structure: Generation of auroral roar fine frequency structure, *J. Geophys. Res.*, *105*, 27,589.

Yoon, P. H., S. Ye, J. LaBelle, A. T. Weatherwax, and J. D. Menietti (2007), Methods in the study of discrete upper hybrid waves, *J. Geophys. Res.*, *112*, A11305, doi:10.1029/2007JA012683.

Zarka, P., B. Cecconi, and W. S. Kurth (2004), Jupiter's low-frequency radio spectrum from Cassini/Radio and Plasma Wave Science (RPWS) absolute flux density measurements, *J. Geophys. Res.*, *109*, A09S15, doi:10.1029/2003JA010260.

B. Cecconi, A. Lecacheux, and P. Zarka, Observatoire de Paris, 92195 Meudon, France. (baptiste.cecconi@obspm.fr; alain.lecacheux@obspm.fr; philippe.zarka@obspm.fr)

G. Fischer, D. A. Gurnett, G. B. Hospodarsky, W. S. Kurth, J. D. Menietti, Z. Wang, and S.-Y. Ye, Department of Physics and Astronomy, University of Iowa, Iowa City, IA 52242 USA. (gf@space.physics.uiowa.edu; donald-gurnett@uiowa.edu; george-hospodarsky@uiowa.edu; william-kurth@uiowa.edu; john-menietti@uiowa.edu; zhenzhen-Wang@uiowa.edu; shengyi-ye@uiowa.edu)